Mapping tree mortality rate in a tropical moist forest using multi-temporal LiDAR

Claudia Huertas, Daniel Sabatier, Géraldine Derroire, Bruno Ferry, Toby Jackson, Raphaël Pélissier, Grégoire Vincent

Mapping tree mortality rate in a tropical moist forest using multi-temporal LiDAR

Claudia Huertas [a,*], Daniel Sabatier [a], Géraldine Derroire [b], Bruno Ferry [c], Toby.D. Jackson [d], Raphaël Pélissier [a], Grégoire Vincent [a,*]

[a] *AMAP, Univ Montpellier, CIRAD, CNRS, INRAE, IRD, Montpellier, France*
[b] *Centre de Coopération Internationale en Recherche Agronomique pour le Développement (CIRAD), 22 UMR EcoFoG (Agroparistech, CNRS, INRAE, Université des Antilles, Université de Guyane), France*
[c] *UMR SILVA, AgroParisTech, INRAE, 54280 Champenoux, France*
[d] *Department of Plant Sciences, University of Cambridge, Downing Street, Cambridge CB2 3EA, France*

ARTICLE INFO

ABSTRACT

Background and aims: Several studies have shown an increase in tree mortality in intact tropical forests in recent decades. However, most studies are based on networks of field plots whose representativeness is debated. We examine the potential of repeated Airborne LiDAR Scanning data to map forest structure change over large areas with high spatial resolution and to detect tree mortality patterns at landscape level.

Methods: The study site is a complex forested landscape in French Guiana with varied topographic positions, vegetation structures and disturbance history. We computed a Gap Dynamics Index from Canopy Height Models derived from successive LiDAR data sets (2009, 2015 and 2019) that we compared to field-measured mortality rates (in stem number and basal area loss) obtained from regular monitoring of 74 1.56-ha permanent plots.

Results: At the plot level, the relation between gap dynamics and absolute basal area loss rate (combining fallen and standing dead trees) was overall highly significant ($R^2 = 0.60$) and especially tight for the 59 ha of unlogged forest ($R^2 = 0.72$). Basal area loss rate was better predicted from gap dynamics than stem loss rate. In particular, in previously logged plots, intense self-thinning of small stems did not translate into detectable gaps, leading to poor predictability of stem mortality by LiDAR in those forests severely disturbed 30 years before. At the landscape scale, LiDAR data revealed spatial patterns of gap creation that persisted over the successive analysis periods. Those spatial patterns were related to local topography and canopy height. High canopy forests and bottomlands were more dynamic, with a higher fraction of canopy affected by gaps per unit time indicating higher basal area loss rates.

Conclusion: Gap detection and mapping via multitemporal LiDAR data is poised to become instrumental in characterizing landscape-scale forest response to current global change. Meaningful comparison of gap dynamics across time and space will, however, depend on consistent LiDAR acquisitions characteristics.

1. Introduction

Evidence for an accelerating global warming trend is accumulating. Each of the last four decades has been successively warmer, with the most significant increase in temperature between 2003 and 2012 ($+0.19\,°C$) (IPCC, In Press). The Amazon, a region considered the richest in terrestrial species (Barlow et al., 2018) and one of the largest global sinks of terrestrial carbon, sequestering ~25% of annual global CO_2 emissions (Brienen et al., 2015; Pan et al., 2011), is also one of the terrestrial areas most vulnerable to global warming (Laurance and Williamson, 2001; Malhi et al., 2008). In this region, a change in precipitation during the transition from the dry to the wet season has been shown to cause trees to die more frequently (Aleixo et al., 2019). In addition, the intensification of extreme events, such as wind-throw, fires, floods or landslides (Gale, 2006), in synergy with human activities (Cochrane and Barber, 2009), intrinsically affects the intensity and

frequency of large-scale mortality (Allen et al., 2015; Leitold et al., 2018; McDowell et al., 2018). Furthermore, over the last decades, change in tree turnover rate has been hypothesized to be a major determinant of the recently documented decline of intact forest C sink (Brienen et al., 2015; Phillips et al., 2008). Therefore, spatial and temporal monitoring of tree mortality rates is of direct relevance to better understand the drivers of mortality and should, in particular, help ascertain if the intact Amazonian forests are still carbon sinks or have become net sources of CO_2 (Brienen et al., 2015; Pan et al., 2011; Vieira et al., 2004).

For decades, these conclusions have been derived from field inventories of networks of permanent field plots (Baker et al., 2021; ForestPlots.net et al., 2021; Malhi et al., 2002). Nevertheless, this approach is limited by inventory plots' representativeness of surrounding landscapes, which is especially critical for the mortality process and impedes drawing robust conclusions by not sufficiently capturing the dynamics of different habitats (Di Vittorio et al., 2014; Marvin et al., 2014). For example, according to a study covering four lowland and six mountain landscapes ranging 500–1.200 ha in size (Marvin et al., 2014), at least 100 1-hectare plots per landscape would be needed to optimally measure above-ground carbon density in heterogeneous landscapes with 90% accuracy, so it would be challenging to have robust and realistic global models covering diverse habitats with currently available networks. Thus, a strategy combining repeated, standardized, and adequately replicated measurements at plot scale with remote sensing approaches to extrapolate at landscape-scale should be prioritized in the coming years (Chave et al., 2019; Kellner and Asner, 2009; Phillips et al., 2016; Réjou-Méchain et al., 2019).

A majority of remote sensing studies that quantify the extent, severity and timing of the disturbance events on the C cycle have been conducted at medium to coarse resolution, varying from a few hundred meters to tens of square kilometers (Xiao et al., 2019). This enables the identification of factors captured at the regional level (Asner and Alencar, 2010). However, higher spatial resolution over large geographic areas in the measurement of biomass primary gross or net production and gap dynamics remains a priority. For example, a study of biomass change in a natural Amazonian forest with multiple plots and remote sensing data sources found that 98.6% of biomass losses correspond to mortality at a small scale (<0.1 ha) (Espírito-Santo et al., 2015). New remote sensing technologies, such as Airborne LiDAR Scanning (ALS), have great potential here as they can detect a change in canopy structure, which can inform about biomass dynamics (Cao et al., 2016; Dubayah et al., 2010; Meyer et al., 2013; Rex et al., 2020) and tree mortality (Dalagnol et al., 2021; Thomas et al., 2013). Another advantage of ALS over other technologies is that it documents terrain elevation as well as canopy structure. Accurate land surface models provide the ability to represent variables associated with local topography and hydrological networks. These variables often co-vary with the structure and dynamics of tropical forests (Coomes et al., 2019; Detto et al., 2013). They have been shown to predict mortality (Campbell et al., 2020), including drought-vulnerable or drought-resistant areas associated with the concept of refuge (orographic wet spots) (Sousa et al., 2020), waterlogged soil that can produce anoxia (Parent et al., 2008), soil fertility related to topography and nutrient deposition (Allié et al., 2015; de Toledo et al., 2011), and treefall vulnerability due to slopes or slope exposure to wind (Alexander et al., 2018). Other advantages offered by ALS technology are the possibility of repeatedly covering large areas, even if remote, that are adequately replicated over relevant spatial scales. ALS can monitor large areas quickly, which is crucial for tracking the demography of millions of trees. ALS can provide data to inform models of forest responses to change (Bustamante et al., 2016; Longo et al., 2020).

Studies exploring tropical forest dynamics from ALS mostly rely on a static definition of gaps (Asner et al., 2013; Asner and Mascaro, 2014; Espírito-Santo et al., 2015) but see (Hunter et al., 2015). However, the relation between gap frequency and mortality is indirect and likely to vary with forest structure. In addition, confounding permanent canopy

openings (clearings, rocky outcrops, etc.) may further blur the expected relation between gap frequency and tree turnover rate. For instance, (Dalagnol et al., 2021) reported an R^2 of 0.7 for a non-linear logarithmic relationship between static gap fraction (%) and annualized dynamic gap fraction (% yr^{-1}) for 5-ha plot areas over five sites in the Brazilian Amazon, suggesting a considerable distortion between the static and dynamic perception of gaps. Studies relating to gap dynamics measured from repeated remote sensing data and ground measurement of tree mortality remain limited in intact tropical forests.

In this study, we use long-term monitoring of 84,675 stems from 115 ha of permanent forest plots to evaluate the ability of repeated ALS data to monitor tree mortality in a complex forest landscape. Dense forests dominate the landscape, including undisturbed plots and plots recovering from past logging conducted in the mid-80s. In particular, we address the following questions:

How tightly correlated are field-observed stem and basal area loss rates with ALS-detected gap dynamics?

How does mortality derived from the ground census vary with local drainage regime, past logging history, and local canopy height?

Do the same factors affect gap dynamics at landscape scale as captured by repeated ALS data?

Is the recent acceleration of mortality observed in undisturbed plots confirmed at the landscape scale using ALS data?

2. Methodology

2.1. Study site and forest inventory data

The study site is Paracou Experimental Station, located in the coastal part of French Guiana (5°18′N − 52°53′). It is covered by lowland rainforest on acrisol soil type with haplic gleysol type (Epron et al., 2006) in hydromorphic bottomlands with a permanent water table. Rainfall is determined by long periods of precipitation (annual mean of 2829 mm during 1980–2019, source Météo France) interrupted by a short dry season in March and a long one from mid-August to mid-November. The climate is described as tropical rainy climate Af in (Köppen classification) with a mean annual temperature of 26.7 °C.

Paracou Experimental Station benefits from an extensive collection of forest inventory and remote sensing data. A network of 15 6.25-ha plots (Fig. 1), submitted to various logging intensities between 1986 and 1988, is surveyed every 1 to 2 years since 1996. Logging intensity has four levels: control plots (unlogged) and plots subjected to silvicultural treatments of increasing intensity (T1 to T3; see Table 1 and (Gourlet-Fleury et al., 2004) for more details). An additional 25-ha unlogged plot established in 1992 is surveyed every five years. In all plots, trees over 10 cm DBH (diameter at breast height, measured at 130 cm above the ground or 50 cm above the buttresses) are regularly measured for girth increment, mortality and recruitment.

From these data, tree mortality was estimated per 125 m × 125 m subplots (~1.56 ha), calculated as the basal area (BA) or stem (Stem) loss from a plot during the studied periods. Relative mortality rates were standardized by the number of live stems or the basal area at the beginning of the observation periods. A subplot of 1.56 ha from one logged plot (P3) was excluded as it lacked data in 2015. These simple mortality rate indicators proved to be robust compared to more sophisticated individual-based models (Kohyama et al., 2018); r = 0.997, p < 0.001.

The logged plots show clear successional dynamics illustrated by an increase in basal area and a simultaneous decrease in stem density over the last two decades. The number of stems is higher in the most severe treatments and remains higher than in the control plots in treatments T2 and T3, 35 years after logging (Fig. 2). A higher frequency of small diameter stems and a lower mean wood density are observed with increasing logging intensity (Appendix 5), both patterns being characteristic of post-harvest successional dynamics. In the rest of the paper, we used information from the 2009, 2015 and 2019 inventories to
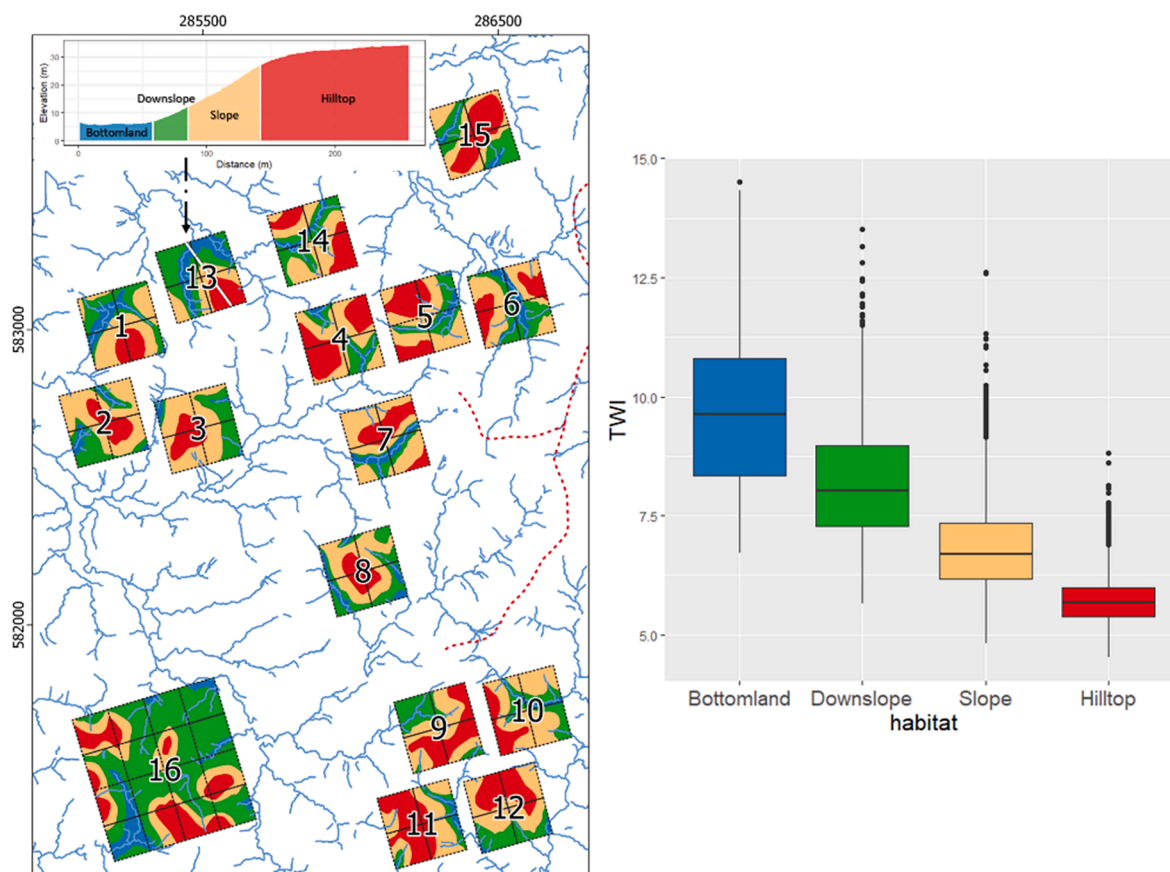
Fig. 1. Left. Map of the study area, showing the different plots and the soil hydrological classes (Habitats; see text). Plot numbers refer to Forest type characteristics summarized in Table 1. Right. Boxplot showing the consistency between Habitat classification and Topographic Wetness Index (TWI) computed over the entire landscape based on the digital terrain model derived from Aerial LiDAR Scanning data (see text).

Table 1
Forest Types definition combining silvicultural treatments of increasing intensity (T1 to T3) and canopy height (HC) for undisturbed plots. Plot numbers refer to Fig. 1. Forest stature was defined from the 2009 Canopy Height Model (CHM) derived from Aerial LiDAR Scanning data as the 90th percentile of pixel-wise CHM values in a 125 m radius (see text). Biomass loss corresponds to the total woody biomass loss attributed to silvicultural treatments (see for details Appendix 1 and (Gourlet-Fleury et al., 2004)).

Forest type	Plot number	Plot area	Mean plot-wise canopy height (HC)	Mean Quadratic Diameter (2015)	Sylvicultural treatment	Harvested biomass
Undisturbed plots						
Short undisturbed forest (SUF)	1,6,11,13,14,15	6.25 ha	28.6 m	25.6 cm	None	0
Tall undisturbed forest (TUF)	16	25 ha	30.8 m	27.6 cm	None	0
Logged plots						
Treatment 1 (T1)	2,7,9	6.25 ha	28.5 m	24.8 cm	Timber	12–33%
Treatment 2 (T2)	3,5,10	6.25 ha	26.7 m	23.2 cm	Timber and Thinning	33–56%
Treatment 3 (T3)	4,8,12	6.25 ha	26.1 m	22.2 cm	Timber, Thinning and Fuelwood	35–56%

compare with the ALS data, except for the 25-ha unlogged plot (P16-Fig. 1), where 2010, 2015 and 2020 censuses were used.

2.2. ALS data and processing

Data from 2009, 2015 and 2019 (Appendix 2) covering a common area of 5.24 km² slightly differed in acquisition characteristics: vehicle (helicopter or airplane), scan angle, flight altitude, pulse rate and LiDAR acquisition mode (single last return in 2009 or multiple returns) - (Appendix 2). In 2009 three different flights were conducted (April, September and October) with two different sensors. The different data sets from 2009 were combined to achieve a relatively high pulse density

(10 pulses.m^{-2}). The other two higher density flights (2015 and 2019) were down-sampled to 10 pulses per m² after restricting the scan angle to +/-20° to increase consistency with 2009 data. Local maximum return height is known to depend on pulse density (Roussel et al., 2017). We found that resampling was necessary as without pulse density standardization gap dynamics estimate (see below) was biased by 10% (Appendix 8).

All point cloud data was processed using LidR package (version 3.2.1 (Roussel and Auty, 2020) in R, except for denoising, which used lasnoise function in Lastools software (version 210128).

To assess canopy change dynamics, a canopy height model (CHM) was calculated from the standardized ALS data points at each date. The
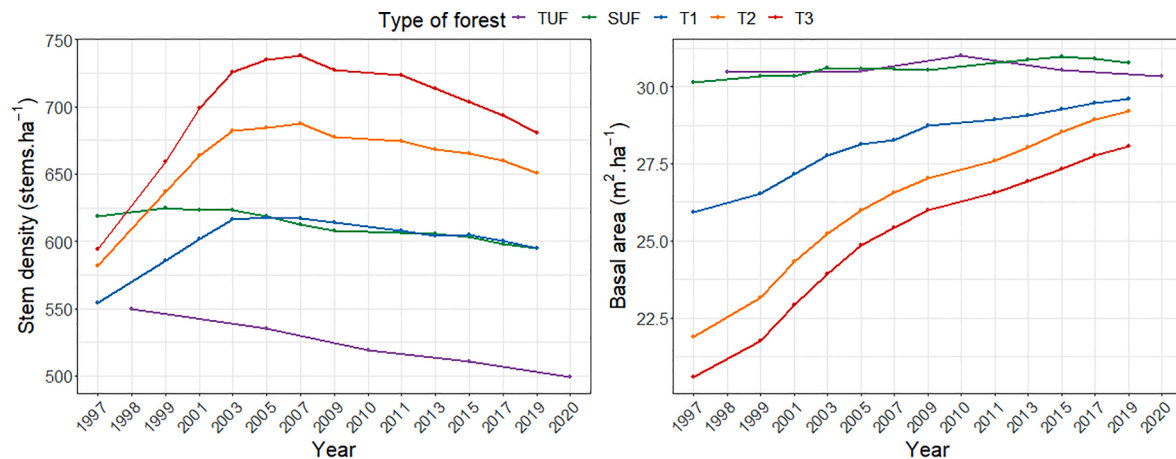
Fig. 2. Mean stem density (stems.ha^{-1}, left) and basal area (BA in m^2.ha^{-1}, right) over 20 years in the different forest types. TUF: Tall Undisturbed Forest; SUF: Short Undisturbed Forest; T1-3: Logged forests of increasing intensity (see ha^{-1} for details).

point cloud was first normalized by subtracting the ground height from the original point cloud measurement. For this purpose, the 2015 digital terrain model calculated with the R package Raster (version 3.4–13 (Hijmans, 2020)) was used for the different dates as it was considered the most accurate (highest density of terrain points). This was equivalent to using differences in the canopy surface model non-normalized by terrain height, since the same terrain model was used for all dates. The height-normalized point clouds were then rasterized with a resolution of 1 m, taking the maximum height of the first returns (Hmax). Hmax was also found to minimize the impact on CHM of leaf density variation (phenology effect), affecting penetration and mean height of returns (Appendix 6 and Appendix 7). We also tested a CHM produced using mean first return height per cell instead of maximum, which proved to be less effective for our analysis.

We also defined a height of canopy variable (HC) as the 90th percentile of pixel-wise CHM 2009 values in a 125x125 m neighborhood. HC should be less sensitive than mean canopy height to gap frequency and to the inclusion of small bottomlands which have a more open canopy (Vincent et al., 2010).

2.3. Gap dynamics index

Gaps were measured dynamically (canopy height loss events) by calculating the difference of CHM between date 1 and date 2. A gap was defined as contiguous pixels affected by a canopy height decrease between two ALS campaigns, larger than a specified threshold. Contiguity was defined in an eight-pixel direction, i.e., including corner contacts. Different thresholds were tested according to different gap detection methods reported in the literature. The various methods (presented in Appendix 4) were assessed by comparison to ground-based mortality rates. The approach of Leitold et al. (2018), defining a minimum gap size of 4 m^2 and a minimum height loss of 3 m between two ALS surveys, showed the highest correlation with field data (r = 0.78, p < 0.001 with absolute BA loss; r = 0.41, p < 0.001 with relative Stem loss). A binary raster image was obtained from mapping gaps formed between successive ALS campaigns. A gap dynamics index (GDI) was computed at the 125-m subplot level as the ratio of total pixels detected as gaps to the total subplot area. This GDI was annualized for comparison with ground-based mortality rates.

For the ten years (2009–2019), the final gap raster was obtained as the combination of gaps newly formed in each of the two intervals 2009–2015 and 2015–2019. Gap opening and closure being a continuous process, the perceived yearly gap fraction will decrease as the time between ALS campaigns increases. For instance, when GDI was estimated directly from the 2009 and 2019 CHMs only, the canopy dynamics was about 20 % lower than estimated per period (2009–2015

and 2015–2019). This bias was more significant in more dynamic plots (Appendix 3).

2.4. Tree mortality and gap dynamics models

We used simple linear models to compare GDI with Stems and BA mortality rates estimated at the plot level (research question 1). To compare the effects of environmental variables on mortality rates and GDI (research questions 2 and 3), which all ranged from 0 to 1, we used generalized linear models (GLM) with a logit link function and a binomial distribution, and homologous independent variables defined at the plot and landscape levels.

At the plot level, stem and BA loss rates were predicted from Habitat and Forest type variables using observation units corresponding to the total area occupied by a habitat class in the 125 × 125 m sampling units. Habitat classes correspond to the four soil hydromorphological categories defined by (Ferry et al., 2010; Morneau, 2007) (Fig. 1): hilltop (flat to gentle slope, soil waterlogging very rare), slope (medium to steep slope, low-intensity waterlogging), downslope (flat to gentle slope, medium-intensity waterlogging) and bottomland (flat, high-intensity waterlogging). These units were delineated based on waterlogging and slope angle (a proxy for soil weathering intensity (Pélissier et al., 2002)). Habitat, defined in this way, was previously identified as a significant factor in predicting spatial variation in mortality rates (Ferry et al., 2010). Forest type combines past disturbance history (logging intensity) and canopy height (HC) information. Plot-wise, mean HC was used to separate undisturbed plots as Short undisturbed forest (SUF) and Tall undisturbed forest (TUF) (see Table 1). Not only do these forests differ in canopy height and Height-Diameter allometry (Vincent et al., 2010; 2014) but also in diameter distribution and dynamics (see Fig. 2 and Appendix 5). These differences in forest stature are suspected to reflect differences in parent material, TUF developing on migmatitic bedrock (Gourlet-Fleury et al., 2004) that tends to be better drained (Schmitt, 1984).

Disturbed forest areas (logged plots, tracks and camps) were masked at landscape level prior to analysis. The elementary observation considered was the 1-meter pixel GDI value (gap vs. non-gap), with HC and a Topographic Wetness Index (TWI) as independent variables. TWI was used to extrapolate at the landscape level the Habitat classification used at the plot level. TWI is widely used in hydrology studies to describe the tendency of an area to accumulate water (Mattivi et al., 2019). It was computed from the digital terrain model derived from ALS data, using the r.topidx tool in the GRASS GIS (version 7.8.2) software, at a resolution of 60 m, then resampled to 10 m using bilinear interpolation. The consistency of TWI and Habitat assessed at 60 m resolution was good despite some overlap in TWI distribution between bottomland

and downslope classes (see boxplot in Fig. 1). To limit spatial autocorrelation effects in the GLM fitted at the landscape level to predict GDI, we did not run the model on the entire set of pixels but instead selected a subset of pixels along a 50 × 50 m grid, so that they can be considered as spatially independent. The grid was randomly located, and the analysis was repeated 100 times. Nested GLMs were ranked using the Akaike Information Criterion (AIC). We also computed the evidence ratio (ER = exp(0.5x∆AIC), which compares the relative likelihood that one model is better than another. All analyses were conducted in R version 3.6.3.

3. Results

3.1. Comparison of gap dynamics and mortality rates within plots

BA and stem loss rate (both absolute and relative) were compared across undisturbed and logged forests to the GDI estimated from ALS data (Fig. 3). BA loss rate was more highly correlated to GDI than stem loss rate. BA relative loss rate was more strongly correlated to GDI than BA absolute loss rate when the analysis was restricted to undisturbed plots (r = 0.85, p = <0.001 vs. r = 0.78, p = <0.001). GDI was moderately correlated with relative but not with absolute stem loss rate when disturbed and undisturbed plots were pooled. The relative stem loss rate was better predicted than the absolute rate due to co-variation in small stem density and mortality rate across the disturbance gradient (see Fig. 2).

Scatter plot of absolute BA loss rate and GDI per forest type illustrates the sensitivity of the relation to disturbance level. When restricted to unlogged plot (SUF and TUF), the relation was particularly strong (R^2 = 0.72, RSE = 0.0032; Fig. 4).

3.2. Mortality and gap dynamics determinants

Relative BA and stem loss rates predicted from the GLMs show similar response patterns to Habitat and Forest Type (Fig. 5). Stem and BA loss rates were predicted to be higher in TUF than SUF and to increase with treatment intensity (T1 to T3). While global responses were similar, there were differences between Forest Types as the relation between both variables (BA and stems) is mediated by stem diameter distribution density which varied across Forest Types (see Quadratic mean diameter in Table 1).

GDI, as predicted from Habitat and Forest Type, matched the patterns modeled from ground data (Fig. 5), with the notable exception of a
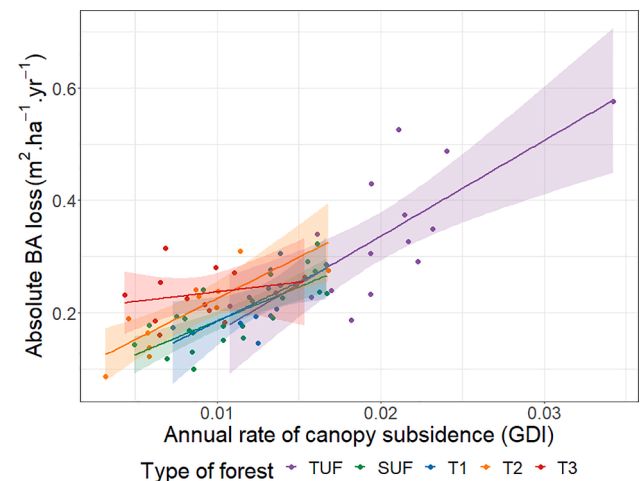

Fig. 4. Absolute basal area loss ($m^2.ha^{-1}.yr^{-1}$) versus GDI (annual rate of canopy subsidence) for 2009–2019 per 125 × 125 m subplot for all types of forests. Regression lines (solid) with a 95% confidence level. TUF: Tall Undisturbed Forest; SUF: Short Undisturbed Forest. T1 to T3: Sylvicultural treatments of increasing intensity (see Table 1 for more details).

low predicted GDI in highly disturbed plots (T2 and T3) and Hilltop habitat.

Differences between predicted stem loss, BA loss and GDI for T2 and T3 result from the peculiar diameter distribution in these severely logged plots, which contain a high abundance of short-lived pioneers with a high mortality from self-thinning of small trees. This mortality is well captured by stem loss predictions, less so by BA loss predictions and not at all by GDI predictions as it does not leave a canopy gap detectable by ALS.

The slight divergence between predictions for Hilltop class was less expected. It reflects a difference in diameter distribution of dead trees between habitats and notably a reduction in mean quadratic diameter on hilltops (Appendix 9).

At a landscape scale, we compared the GLM predictions of GDI with TWI and HC (Fig. 6) effects separately or together, including their interaction. The analysis was repeated 100 times (see M&M). The best model included both predictors without interaction (Table 2).

As a complement, the spatial cross-correlation between individual 1-

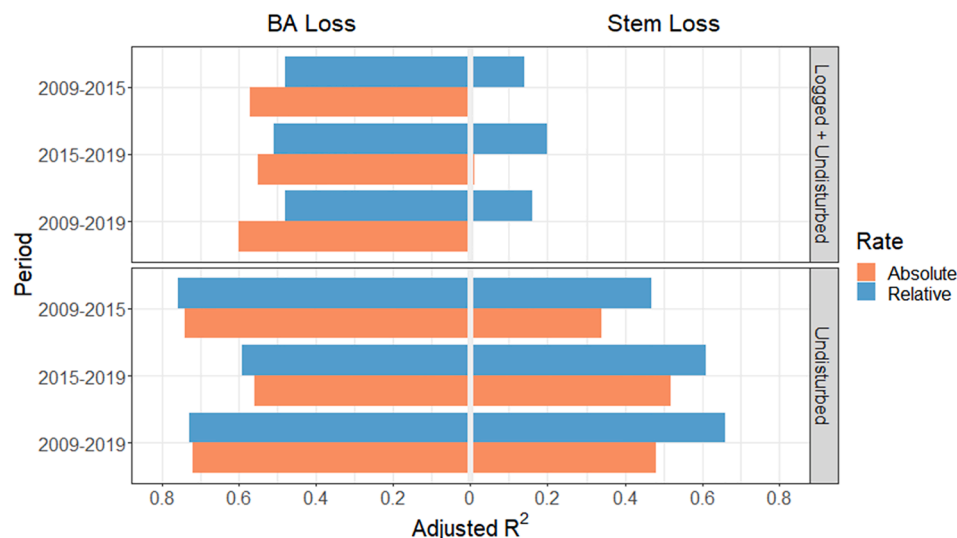**Fig. 3.** Adjusted R-squared of the linear regression between GDI and BA or stem loss rates according to different periods. Absolute loss rates in red and relative loos rates in blue. Upper graphs include all plots, and lower graphs include only undisturbed plots. (For interpretation of the references to colour in this figure legend, the reader is referred to the web version of this article.)
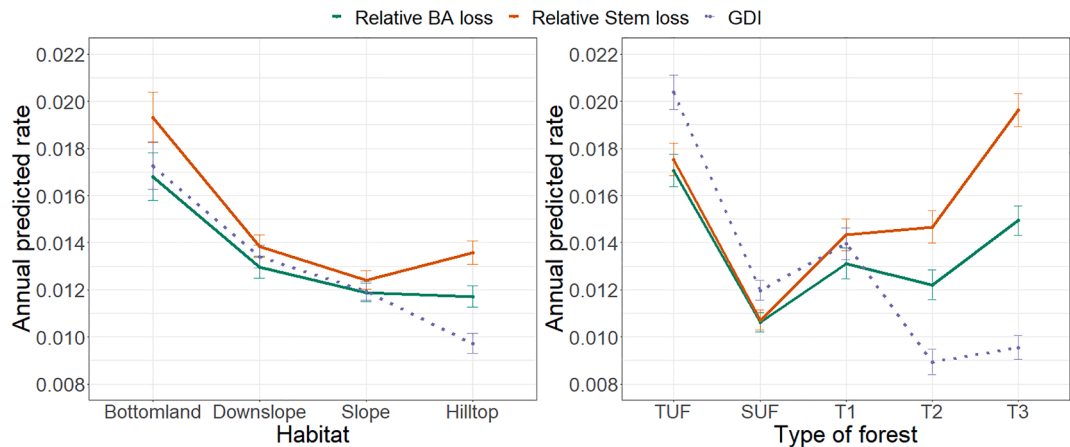
Fig. 5. Effect of Habitat and Forest type (TUF = Tall Undisturbed Forest, SUF = Short Undisturbed Forest, T1-T3 = increasing level of logging intensity) on annual basal and stem loss rates predicted for the period 2009–2019 per hectare. Error bars represent 95% confidence limits.
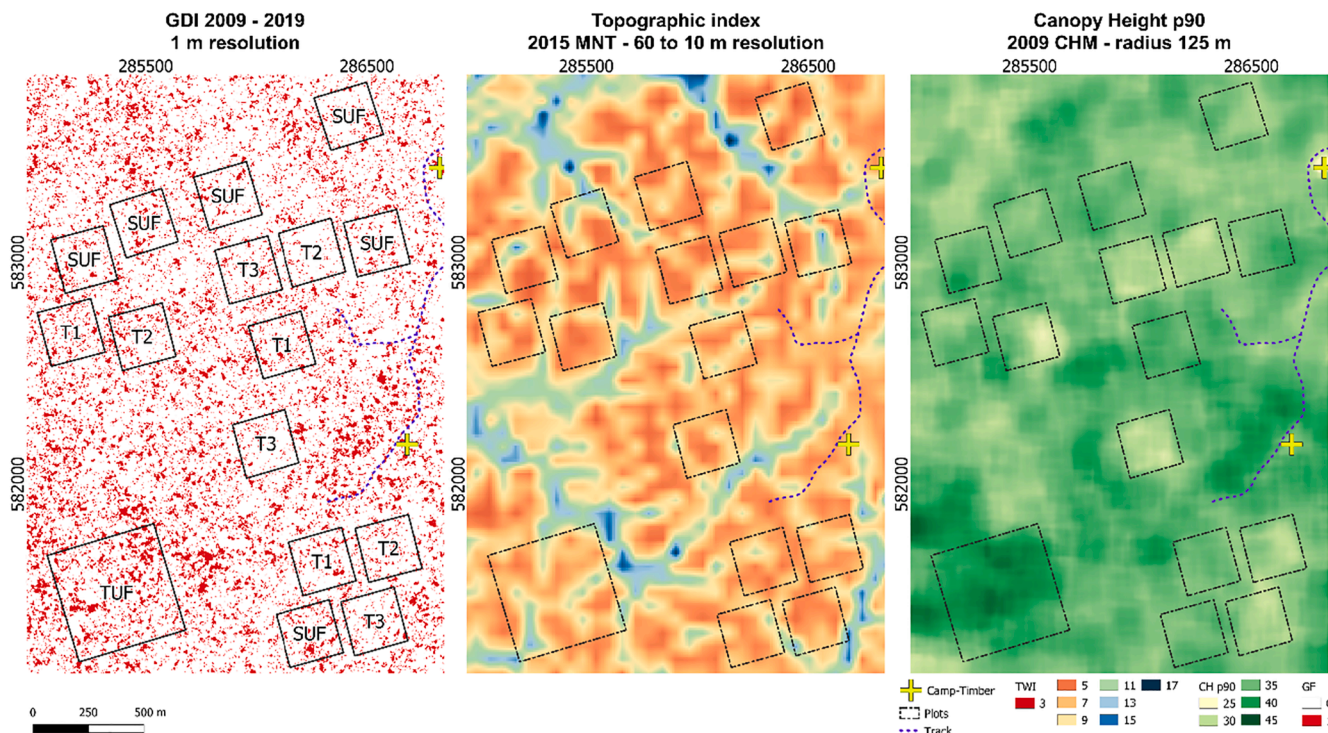

Fig. 6. a) GDI per pixel of 1 m. b) TWI (calculated at 60 m, resampled at 10 m. c) and canopy height (HC) taken as the 90th percentile (p90) of 1-m CHM period 2009 values in a 125 m radius neighborhood.

Table 2
Median values of statistics of nested models of gap dynamic index computed at 1 m pixel for 100 random pixel selections.

Model	GDI ~ TWI + HC	GDI ~ HC	GDI ~ TWI	GDI ~ HC*TWI
Median AIC	1162.74	1174.45	1170.25	1164.37
Median Evidence Ratio	–	299.7	40.3	2.24

m pixel values of TWI and GDI over undisturbed areas (i.e., logged plots, tracks and camp masked) was equal to r = 0.35 (P < 0.001 - torus translation test; (Harms et al., 2001)). On the other hand, the correlation between HC and GDI was 0.40 (P < 0.001 - torus translation test; (Harms et al., 2001)).

3.3. Temporal changes in mortality detection with ALS

We tested spatial cross-correlation of GDI overtime at landscape-level and observed a significant correlation between the periods 2009–2015 and 2015–2019 (Fig. 7) (r = 0.50, p = <0.001, torus translation test).

Mean and median absolute BA and stem loss increased in the undisturbed forest at the 125-m subplot level between 2009 and 2015 and 2015–2019. Mean change in BA relative loss rate, stem relative loss rate and GDI were 14%, 12% and 9%, respectively (Fig. 8). A Wilcoxon signed-rank test concluded to a significant change over time for BA (Z = 268, p = 0.028) and stem (Z = 238, p = 0.011) but not for GDI (Z = 340, p = 0.177).

The increase in BA and stem mortality rate between 2009 and 2015 and 2015–2019 was higher in short (SUF) than in tall (TUF) forests
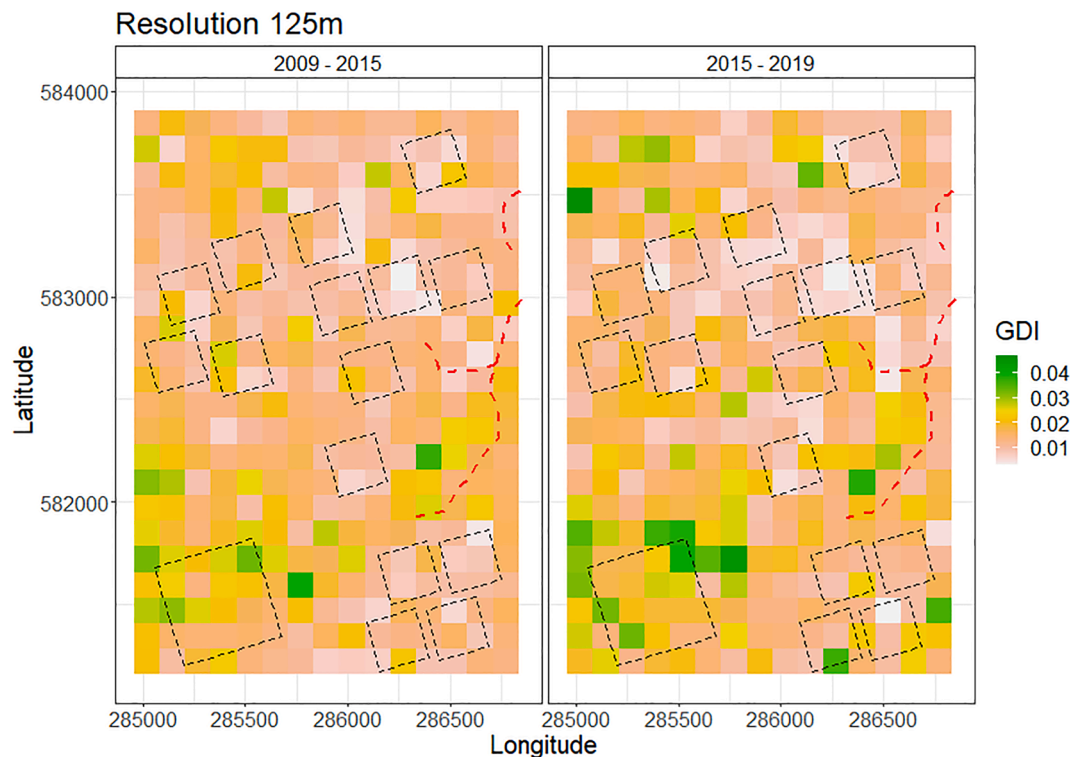
Fig. 7. Map of a Gap Dynamics Index derived from repeated Aerial LiDAR Scanning data in two successive periods: 2009–2015 and 2015–2019, showing a persistent spatial pattern.
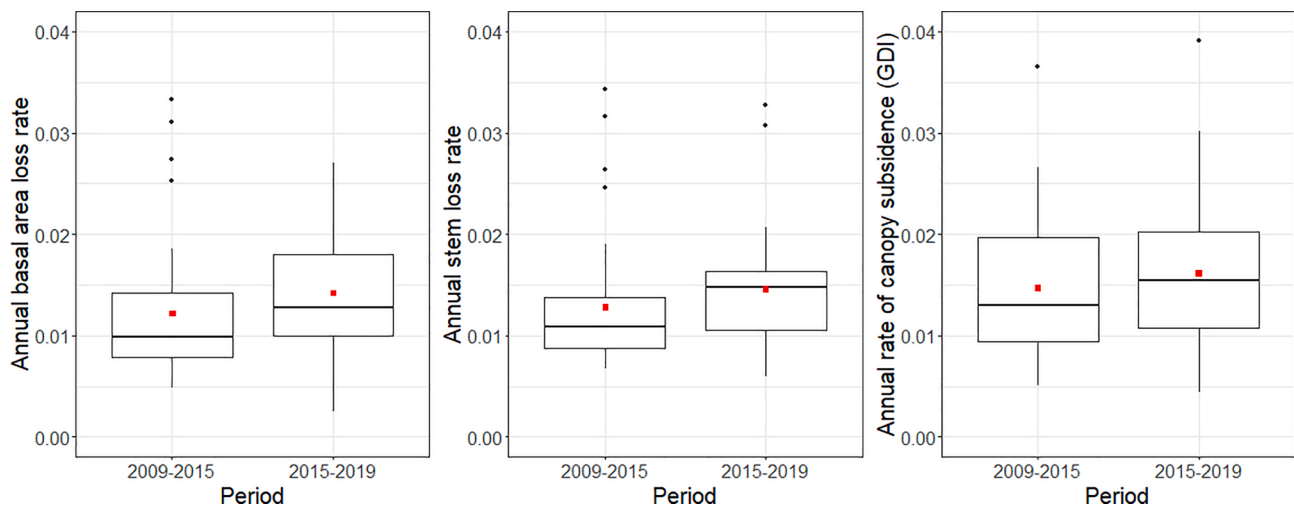

Fig. 8. Mortality (BA and stem loss rates) and gap dynamics index GDI (annual rate of canopy subsidence) derived from repeated Aerial LiDAR Scanning data for different study periods (unlogged plots only). The red dots correspond to the mean value. (For interpretation of the references to colour in this figure legend, the reader is referred to the web version of this article.)

(+19% vs. + 10%, and + 28% vs. + 8%, respectively for BA and stem).

Masking all field plots and disturbed areas (tracks and camps), we found a slight increase (+6%) in GDI during the second period, albeit lower than the change in GDI observed within undisturbed plots (+9%). Differences between periods were, however, not statistically significant (Wilcoxon's signed-rank test: p = 0.82).

4. Discussion

4.1. Gap dynamics is strongly related to BA loss rate across all forest types

We found that gap dynamics *sensu* (Leitold et al., 2018) was

generally well correlated to mortality rates at 125 m resolution. The strength of this correlation nonetheless varied with the mortality rates indicators considered: relative or absolute loss rates expressed on a stem or BA basis. When restricted to undisturbed forest plots, the relation between mortality rates and the gap dynamics index (GDI) was high (R^2 = 0.72 and 0.49 for absolute basal area and stem loss rates, respectively), but it decreased significantly when logged plots were included (Fig. 3). Correlation was typically higher for relative BA loss rates than relative stem loss rates because ALS is more sensitive to the death of large trees. Failure to predict the number of stems lost per unit area resulted from many more small stems undetected by ALS dying in logged plots (Appendix 5). Conversely, when expressed in terms of basal area

loss, the smaller basal area in logged plots increased the discrepancy between GDI and basal area loss expressed in relative terms.

These results indicate that the canopy height model derived from repeated ALS was not sensitive to subcanopy trees mortality. Hence, gap frequency cannot be considered a robust proxy of stem mortality rates across a landscape including mature stands recovering from recent disturbance with accelerated demographic rates. However, the correlation with basal area loss appears to be much more stable and carbon flux monitoring from repeated ALS remains a valid option.

4.2. Spatial and temporal variation in mortality rates

Analysis at the landscape level (excluding logged plots) showed significantly correlated spatial patterns of GDI in two successive periods (r = 0.48 60 m resolution 2009–2015, 2015–2019). Those persistent spatial patterns of canopy dynamics were related to differences in local drainage (TWI) and forest stature (HC) (Fig. 6) and the effects of these two variables appeared to be additive (Table 2). Similar response patterns of GDI to Habitat and HC were observed at the plot level (Fig. 5, undisturbed forest).

Habitat effects on tree mortality had already been documented at the plot scale on this site (Ferry et al., 2010; Morneau, 2007). We extended those results to the tall forest (TUF) and logged forest (Fig. 5). Thanks to ALS, mortality patterns in relation to forest height and local drainage were further confirmed to exist at a larger spatial scale (>5 km^2) across undisturbed forest types.

The acceleration in yearly GDI from 2009 to 2015 to 2015–2019 (+9%) was not as strong as the acceleration in mortality rates observed in ground data (+14% increase in BA loss rate). This may be due to several limitations in the data used here.

4.3. Limitations in the current study

The observed relation between basal area loss and GDI may be blurred by the imperfect match between ground inventories' monitoring dates and ALS campaigns. For instance, TUF (plot 16), ground data were collected in 2010 and 2020, while ALS was acquired in 2009 and 2019 and we know from a previous study at the same site (Vincent et al., 2012) that a 1-yr time lag between ground and ALS data can result in c. 1% uncertainty in LiDAR-derived BA estimations. We decided nevertheless to keep this plot in the present study because its structure and dynamics differed markedly from SUF. This brought more significance to the findings presented by including a more diverse set of forest types.

Another source of temporal mismatch stemmed from the long time span over which ground censuses extend (it takes up to six months to complete the measurement of all 16 plots) compared to the few hours it takes to complete an ALS overflight covering all plots. To further complicate matters, the exact ground census date was not available for each plot every year. This introduced uncertainty in ground-based estimates of mortality rates.

ALS data used in the present study was not devoid of limitations of their own. Differences in ALS acquisition characteristics between 2009 and subsequent dates other than point density and scan angle could not be mitigated. These included footprint size, penetration and single last vs. multiple return modes (Appendix 2). This may notably have affected the temporal comparison between 2009 and 2015 and 2015–2019. Therefore, the net effect of the differing LiDAR system characteristics on CHM differences is difficult to assess. Another significant source of uncertainty affecting the 2009 pooled data set may come from mixing data acquired at six-month intervals (in different seasons).

Deriving CHM from the local maximum height (rather than the mean return height, for instance) made the CHM fairly robust to differences in penetration or scanning angle (Appendix 6). It also allowed seasonal leaf loss not to be confused with gap creation (Appendix 7). Conversely, defoliation, which may also be an early sign of tree death, will not be picked up.

ALS may also fail to detect standing dead trees in the upper canopy until they undergo a significant degree of decay which may take months or even years. For example, in Paracou, 48% of the trees dying from 1991 to 2020 in SUF plots have been recorded as dying standing.

False-positive errors may occur as well. Large branch fall, stem breakage without tree death, partial die-back may all generate a local change in CHM that our indicator may pick up while not associated with tree death. Such events are probably frequent and of significant magnitude, as suggested by previous studies (Chambers et al., 2001; Chave et al., 2003; van der Meer and Bongers, 1996).

4.4. Future research directions

Detecting the change in canopy structure not affecting the uppermost canopy would have required using the entire point cloud rather than a surface model extracted from the point cloud. At least two different strategies could be considered: individual tree death detection and change in estimated plant area density. However, both strategies suffer from methodological limitations due to the lack of accuracy of 3D information below the canopy, as the ALS signal is rapidly attenuated through the vegetation layers (Vincent et al., 2017). A solution to better describe below canopy structure may be to massively increase sampling density while using an extremely narrow laser beam (low flying UAV LiDAR System for instance). Monitoring tree death below the canopy would further require detecting, segmenting, and ideally tracking individual tree crowns over time. Individual crown monitoring and frequent overflights would further allow detecting permanently leafless dead crowns, improving detection of trees dying standing. Indeed, leaflessness can readily be detected in high-density point clouds (Appendix 7). While progress is being made in 3D individual tree crown segmentation in ALS point cloud (Aubry-Kientz et al., 2021; 2019), reliable segmentation of non-dominant or non-emergent trees is still a difficult task in dense multi-layered forests since spectral information which is needed to individualize crowns is restricted to the sunlit upper canopy.

5. Conclusions

This study demonstrated that multitemporal ALS can produce reliable estimates of relative and absolute basal area loss and stem mortality rates in natural forests and confirmed the ability of ALS to detect previously identified patterns of mortality rates related to local topography and its association with terrain wetness index. Mortality rates expressed as basal area loss rates were generally better predicted than stem mortality loss rates, especially in severely disturbed plots. Gap dynamics can help track change in forest carbon fluxes and should usefully complement carbon net change monitoring derived from static carbon estimates modeled from ALS at different dates. Standardization of ALS acquisition parameters across dates (and sites) is a prerequisite for drawing meaningful comparisons. It is also essential to compare periods of similar duration due to the dynamic nature of gap creation and closure. If such conditions are met, repeated ALS should effectively detect and map possible changes in mortality rates triggered by climatic change.

The fine description of the spatial organization of canopy dynamics may further help identify likely environmental drivers of the variability of forest turnover rates, even if, as evidenced in the present paper, absolute estimations of mortality rates from ALS data are still tainted with uncertainty. In addition, wall-to-wall maps of canopy gap dynamics will inform about the representativeness of existing plots.

CRediT authorship contribution statement

Claudia Huertas: Conceptualization, Investigation, Formal analysis, Writing – original draft. **Daniel Sabatier:** Conceptualization, Writing – review & editing. **Géraldine Derroire:** Resources, Writing – review & editing. **Bruno Ferry:** Writing – review & editing. **Toby.D. Jackson:** Writing – review & editing. **Raphaël Pélissier:** Writing – review &

editing. **Grégoire Vincent:** Conceptualization, Investigation, Writing – original draft, Supervision.

Declaration of Competing Interest

The authors declare that they have no known competing financial interests or personal relationships that could have appeared to influence the work reported in this paper.

Acknowledgments

We gratefully acknowledge funding by "Investissement d'Avenir"

Appendix 1. Silvicultural treatments implemented on the plots in Paracou. The number of individuals dead under "silviculture" heading includes dead trees following forest treatment (timber, fuelwood, and thinning) and trees destroyed by forest works. Adapted from: [72] .

Intensity	Plots	Treatments implemented Timber	Trees dead Fuelwood	Thinning	Felled	Logging	Poison-girdling	Silviculture	Canopy height increase* (m ha^{-1} yr^{-1})
T0: SUF	1,6,11,13,14,15				0	0	0	0	0.15
T1:Low intensity	2,7,9	DBH ≥ 50 or 60 cm			3.3	2.3	0	5.6	0.19
T2: Medium intensity	3,5,10	DBH ≥ 50 or 60 cm		DBH ≥ 40 cm	3.8	2.6	5.2	11.6	0.23
T3: Heavy intensity	4,8,12	DBH ≥ 50 or 60 cm	40 cm ≤ DBH ≤ 50 cm	DBH≥50 cm	6.3	4.2	3.6	14.1	0.24
P16: 25 ha plot – TUF	16				0	0	0	0	

* Measured from 2009 and 2019 canopy models.

Appendix 2. . Characteristics of ALS acquisitions for the different overflights.

Year	2009	2015	2019
Acquisition time	April, September, October 2009	20th October 2015	November 2019
Vehicle	Helicopter	Airplane	Airplane
Sensor model	Riegl LMS-280i / LMS6Q140i-60	LMS-Q780 RIEGL (12% power)	LMS-Q780 RIEGL (25% power)
Laser beam divergence (mrad)	≤0.5 mrad/≤3.0 mrad	≤ 0.25	≤ 0.25
Average point density (pulses m^{-2})	10	10 (25*)	10 (27*)
Maximum scan angle	15°	20°	20°
Average flying altitude (m)	170	800	800
Mean footprint size (cm)	10 / 40	20	20
Penetration**	0.009	0.020	0.024

*Initial pulse density (before thinning).

** ground last return divided by all last returns; calculated after excluding shots outside ± 15° angular range.

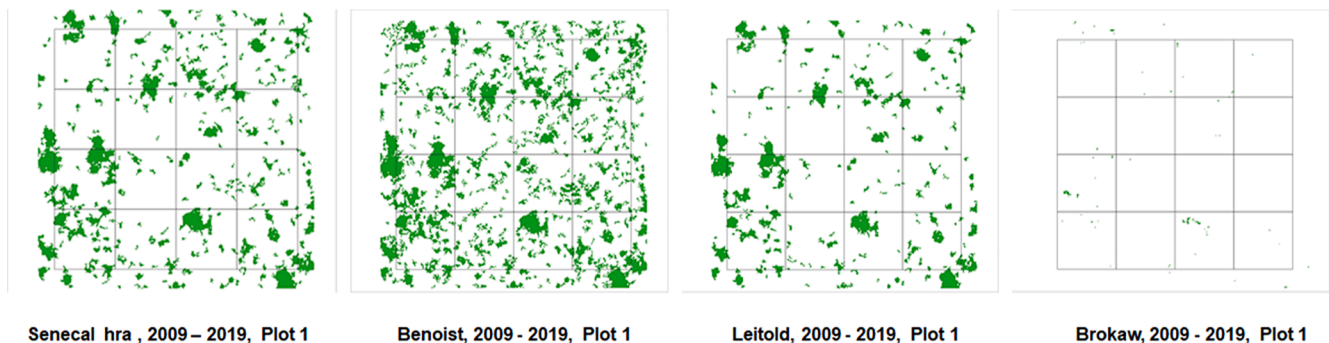**Appendix 3. . Comparison of the GDI indicator calculated, i.e., using 2009 and 2019 as inputs, and the composite as the sum of GDI 2009–2015 and 2015–2019 for all plots (75 subplots).**


$$y = -0.0094 + 0.91 \cdot x, \ R^2 = 0.97$$
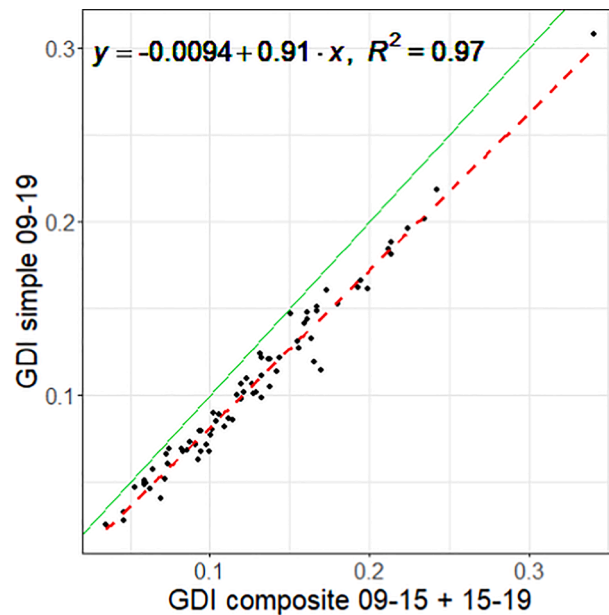
Note: Gaps detected in 2015–2019, also detected in 2009–2015 represented 3.6% of the total gap areas formed between 2009 and 2019.

Appendix 4. . Visual comparison of the different methodologies used for the detection of mortality from gap dynamics analysis. (Benoist, 2009; Brokaw, 1985; Leitold et al., 2018; Senécal et al., 2018)

Senecal hra , 2009 – 2019, Plot 1 | Benoist, 2009 - 2019, Plot 1 | Leitold, 2009 - 2019, Plot 1 | Brokaw, 2009 - 2019, Plot 1

- Brokaw (1982) – Aperture extending at all levels up to an average height of 2 m above the ground.
- Benoist (2009) developed an algorithm to detect and delimit gaps. "The threshold of 5 m^2 minimum makes it possible to exclude low points that are too isolated and that correspond to old gaps that are in the process of aggradation. On the other hand, the 10 m height criterion restores their shape well, and it is reasonable to accept a high point in the middle of a hole."
- (Senécal et al., 2018). Height reduction areas (HRA) groups of pixels in which a reduction of at minimum 1 m in height and a minimum size of 5 m^2 were observed (six years). Within the HRA, new gap pixels were detected as CHM year1 pixels in the HRA of height 3 m or less, and for year0 heights above 3 m, while canopy height erosion pixels were detected as CHM year1 pixels of height above 3 m after the height loss.
- Leitold et al., (2018), threshold >= 4 m^2 and height losses >= 3 m.

Appendix 5. . *Dynamic characteristics per forest type during 2009–2019 (2010–2020)* (a) diameter distribution of trees that died; bins of 10 cm starting at 10 cm dbh. (b) mean value of wood density for surviving, dying and recruited trees (c) demographic rates were calculated as instantaneous rates in SUF plots, logged plots (T1 to T3) between 1999 and 2019 and TUF between 2010 and 2020 for individuals with DBH>=10 cm. Circles for medians, vertical bars for 95% highest posterior distribution intervals, and horizontal axis dotted for y = 0.
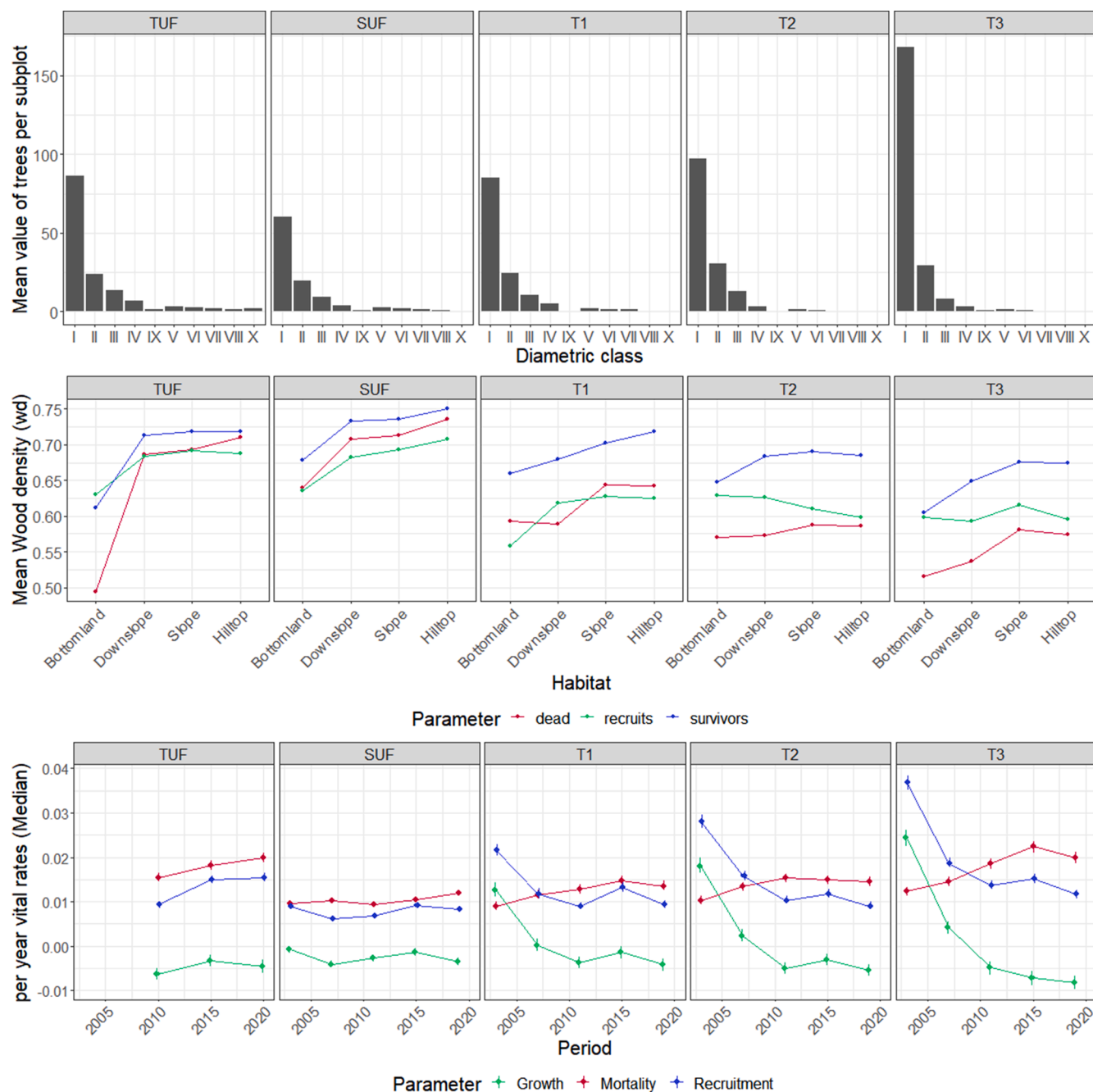
Appendix 6. . Pseudo change (noise) in canopy height evaluated at one m resolution from two flights (05/10/2015 and 20/10/2015) in Paracou. The scan angle was limited to +/- 20 deg. Pulse density was 10 pulses.m^2.
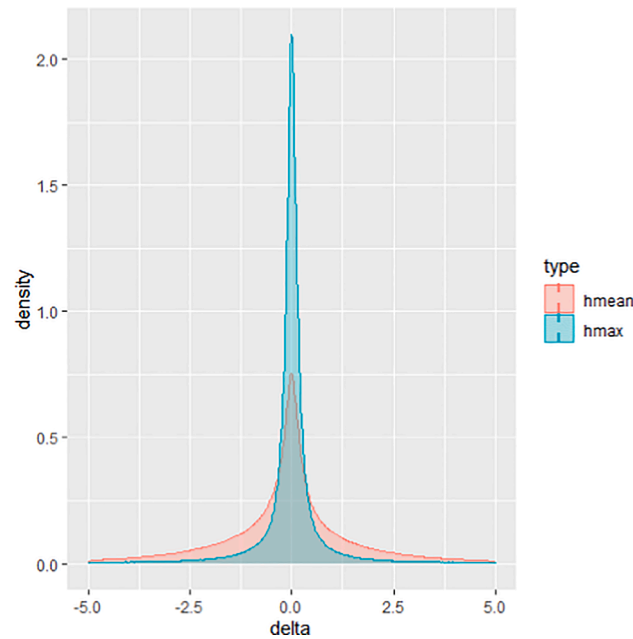
Appendix 7. . Impact of change in leaf density (phenology) on canopy height model occurring over two weeks (05/10/2015 and 20/10/ 2015, Paracou - French Guiana).

In the upper left corner: a crop of the 20/10/2015 Canopy Height Model based on mean first return height (CHM_hmean). In the lower-left corner: the Canopy Height model based on maximum first return height (CHM_hmax, used in the present study), for the same area, same date exact resolution. In the center: raster of change between the two dates. Two crowns (green and red boxes) are highlighted. A significant increase in CHM_hmean is perceptible for those crowns. On the right: Pictures (20/10/2015) of those crowns show that they were re-foliating on the second date. CHM_hmax is not sensitive to such phenology-related changes in the canopy. In addition, CHM_hmean seems spatially more variable, with significant contrasts often associated with gaps.
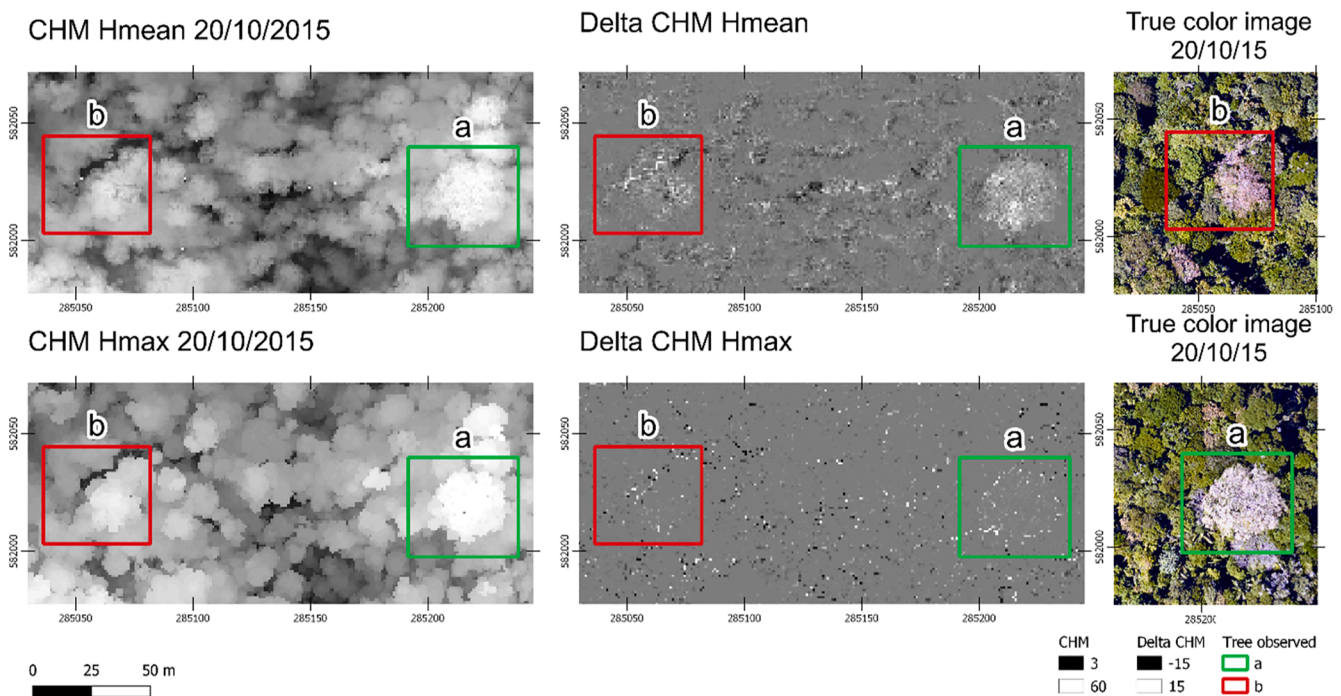
Appendix 8. . Sensitivity of gap fraction to unbalanced pulse density between dates
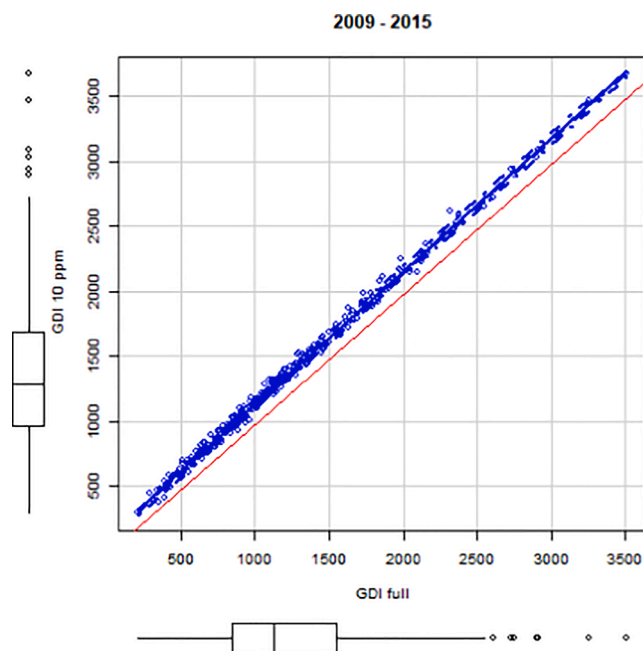
Area in gaps detected using Leitold gap definition (nobs = 321) per 125x125 m cell. Mean difference in gap area is 134 m^2.

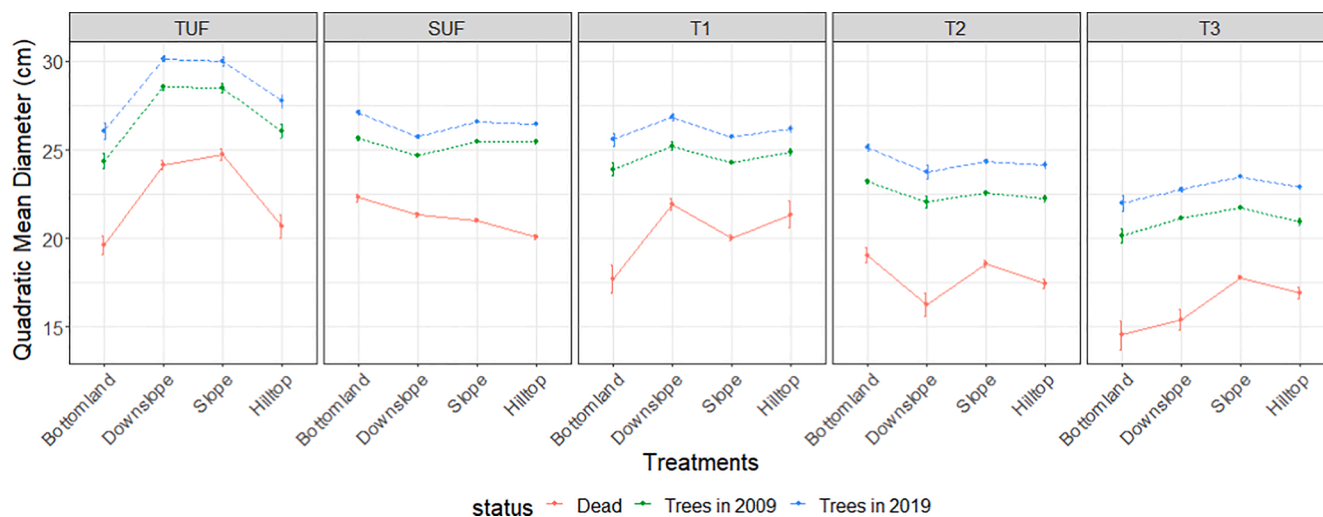**Appendix 9. . Quadratic mean diameter (QMD in cm) per Habitat and forest Type. The vertical bars represent the standard error of the mean per subplot.**

References

Aleixo, I., Norris, D., Hemerik, L., Barbosa, A., Prata, E., Costa, F., Poorter, L., 2019. Amazonian rainforest tree mortality driven by climate and functional traits. Nat. Clim. Change 9, 384–388. https://doi.org/10.1038/s41558-019-0458-0.

Alexander, C., Korstjens, A.H., Hill, R.A., 2018. Influence of micro-topography and crown characteristics on tree height estimations in tropical forests based on LiDAR canopy height models. Int. J. Appl. Earth Obs. Geoinformation 65, 105–113. https://doi.org/10.1016/j.jag.2017.10.009.

Allen, C.D., Breshears, D.D., McDowell, N.G., 2015. On underestimation of global vulnerability to tree mortality and forest die-off from hotter drought in the Anthropocene. Ecosphere 6, art129. https://doi.org/10.1890/ES15-00203.1.

Allié, E., Pélissier, R., Engel, J., Petronelli, P., Freycon, V., Deblauwe, V., Soucémarianadin, L., Weigel, J., Baraloto, C., 2015. Pervasive Local-Scale Tree-Soil Habitat Association in a Tropical Forest Community. PLoS ONE 10, e0141488. https://doi.org/10.1371/journal.pone.0141488.

Asner, G.P., Alencar, A., 2010. Drought impacts on the Amazon forest: the remote sensing perspective: Research review. New Phytol. 187, 569–578. https://doi.org/10.1111/j.1469-8137.2010.03310.x.

Asner, G.P., Kellner, J.R., Kennedy-Bowdoin, T., Knapp, D.E., Anderson, C., Martin, R.E., 2013. Forest Canopy Gap Distributions in the Southern Peruvian Amazon. PLoS ONE 8, e60875. https://doi.org/10.1371/journal.pone.0060875.

Asner, G.P., Mascaro, J., 2014. Mapping tropical forest carbon: Calibrating plot estimates to a simple LiDAR metric. Remote Sens. Environ. 140, 614–624. https://doi.org/10.1016/j.rse.2013.09.023.

Aubry-Kientz, M., Dutrieux, R., Ferraz, A., Saatchi, S., Hamraz, H., Williams, J., Coomes, D., Piboule, A., Vincent, G., 2019. A Comparative Assessment of the Performance of Individual Tree Crowns Delineation Algorithms from ALS Data in Tropical Forests. Remote Sens. 11, 1086. https://doi.org/10.3390/rs11091086.

Aubry-Kientz, M., Laybros, A., Weinstein, B., Ball, J.G.C., Jackson, T., Coomes, D., Vincent, G., 2021. Multisensor Data Fusion for Improved Segmentation of Individual Tree Crowns in Dense Tropical Forests. IEEE J. Sel. Top. Appl. Earth Obs. Remote Sens. 14, 3927–3936. https://doi.org/10.1109/JSTARS.2021.3069159.

Baker, T.R., Vicuña Miñano, E., Banda-R, K., Castillo Torres, D., Farfan-Rios, W., Lawson, I.T., Loja Alemán, E., Pallqui Camacho, N., Silman, M.R., Roucoux, K.H., Phillips, O.L., Honorio Coronado, E.N., Monteagudo Mendoza, A., Rojas Gonzáles, R., 2021. From plots to policy: How to ensure long-term forest plot data supports environmental management in intact tropical forest landscapes. PLANTS PEOPLE PLANET 3, 229–237. https://doi.org/10.1002/ppp3.10154.

Barlow, J., França, F., Gardner, T.A., Hicks, C.C., Lennox, G.D., Berenguer, E., Castello, L., Economo, E.P., Ferreira, J., Guénard, B., Gontijo Leal, C., Isaac, V., Lees, A.C., Parr, C.L., Wilson, S.K., Young, P.J., Graham, N.A.J., 2018. The future of hyperdiverse tropical ecosystems. Nature 559, 517–526. https://doi.org/10.1038/s41586-018-0301-1.

Benoist, V., 2009. Étude de la mortalité des arbres en forêt tropicale humide par laser aéroporté.

Brienen, R.J.W., Phillips, O.L., Feldpausch, T.R., Gloor, E., Baker, T.R., Lloyd, J., Lopez-Gonzalez, G., Monteagudo-Mendoza, A., Malhi, Y., Lewis, S.L., Vásquez Martinez, R., Alexiades, M., Álvarez Dávila, E., Alvarez-Loayza, P., Andrade, A., Aragão, L.E.O.C., Araujo-Murakami, A., Arets, E.J.M.M., Arroyo, L., Aymard, C., G.A., Bánki, O.S., Baraloto, C., Barroso, J., Bonal, D., Boot, R.G.A., Camargo, J.L.C., Castilho, C.V., Chama, V., Chao, K.J., Chave, J., Comiskey, J.A., Cornejo Valverde, F., da Costa, L., de Oliveira, E.A., Di Fiore, A., Erwin, T.L., Fauset, S., Forsthofer, M., Galbraith, D.R., Grahame, E.S., Groot, N., Hérault, B., Higuchi, N., Honorio Coronado, E.N., Keeling, H., Killeen, T.J., Laurance, W.F., Laurance, S., Licona, J., Magnussen, W.E., Marimon, B.S., Marimon-Junior, B.H., Mendoza, C., Neill, D.A., Nogueira, E.M., Núñez, P., Pallqui Camacho, N.C., Parada, A., Pardo-Molina, G., Peacock, J., Peña-Claros, M., Pickavance, G.C., Pitman, N.C.A., Poorter, L., Prieto, A., Quesada, C.A., Ramírez, F., Ramírez-Angulo, H., Restrepo, Z., Roopsind, A., Rudas, A., Salomão, R. P., Schwarz, M., Silva, N., Silva-Espejo, J.E., Silveira, M., Stropp, J., Talbot, J., ter Steege, H., Teran-Aguilar, J., Terborgh, J., Thomas-Caesar, R., Toledo, M., Torello-Raventos, M., Umetsu, R.K., van der Heijden, G.M.F., van der Hout, P., Guimarães Vieira, I.C., Vieira, S.A., Vilanova, E., Vos, V.A., Zagt, R.J., 2015. Long-term decline of the Amazon carbon sink. Nature 519, 344–348. 10.1038/nature14283.

Brokaw, N.V.L., 1985. Gap-Phase Regeneration in a Tropical Forest. Ecology 66, 682–687. https://doi.org/10.2307/1940529.

Bustamante, M.M.C., Roitman, I., Aide, T.M., Alencar, A., Anderson, L.O., Aragão, L., Asner, G.P., Barlow, J., Berenguer, E., Chambers, J., Costa, M.H., Fanin, T., Ferreira, L.G., Ferreira, J., Keller, M., Magnusson, W.E., Morales-Barquero, L., Morton, D., Ometto, J.P.H.B., Palace, M., Peres, C.A., Silvério, D., Trumbore, S., Vieira, I.C.G., 2016. Toward an integrated monitoring framework to assess the effects of tropical forest degradation and recovery on carbon stocks and biodiversity. Glob. Change Biol. 22, 92–109. https://doi.org/10.1111/gcb.13087.

Campbell, M.J., Dennison, P.E., Tune, J.W., Kannenberg, S.A., Kerr, K.L., Codding, B.F., Anderegg, W.R.L., 2020. A multi-sensor, multi-scale approach to mapping tree mortality in woodland ecosystems. Remote Sens. Environ. 245, 111853 https://doi.org/10.1016/j.rse.2020.111853.

Cao, L., Coops, N.C., Innes, J.L., Sheppard, S.R.J., Fu, L., Ruan, H., She, G., 2016. Estimation of forest biomass dynamics in subtropical forests using multi-temporal airborne LiDAR data. Remote Sens. Environ. 178, 158–171. https://doi.org/10.1016/j.rse.2016.03.012.

Chambers, J.Q., dos Santos, J., Ribeiro, R.J., Higuchi, N., 2001. Tree damage, allometric relationships, and above-ground net primary production in central Amazon forest. For. Ecol. Manag. 152, 73–84. https://doi.org/10.1016/S0378-1127(00)00591-0.

Chave, J., Condit, R., Lao, S., Caspersen, J.P., Foster, R.B., Hubbell, S.P., 2003. Spatial and temporal variation of biomass in a tropical forest: results from a large census plot in Panama. J. Ecol. 91, 240–252. https://doi.org/10.1046/j.1365-2745.2003.00757.x.

Chave, J., Davies, S.J., Phillips, O.L., Lewis, S.L., Sist, P., Schepaschenko, D., Armston, J., Baker, T.R., Coomes, D., Disney, M., Duncanson, L., Hérault, B., Labrière, N., Meyer, V., Réjou-Méchain, M., Scipal, K., Saatchi, S., 2019. Ground Data are Essential for Biomass Remote Sensing Missions. Surv. Geophys. 40, 863–880. https://doi.org/10.1007/s10712-019-09528-w.

Cochrane, M.A., Barber, C.P., 2009. Climate change, human land use and future fires in the Amazon. Glob. Change Biol. 15, 601–612. https://doi.org/10.1111/j.1365-2486.2008.01786.x.

Coomes, D., Disney, M., Burslem, D., Jackson, T., 2019. A 3D perspective on the effects of topography and wind on forest height and dynamics.

Dalagnol, R., Wagner, F.H., Galvão, L.S., Streher, A.S., Phillips, O.L., Gloor, E., Pugh, T.A. M., Ometto, J.P.H.B., Aragão, L.E.O.C., 2021. Large-scale variations in the dynamics of Amazon forest canopy gaps from airborne lidar data and opportunities for tree mortality estimates. Sci. Rep. 11, 1388. https://doi.org/10.1038/s41598-020-80809-w.

de Toledo, J.J., Magnusson, W.E., Castilho, C.V., Nascimento, H.E.M., 2011. How much variation in tree mortality is predicted by soil and topography in Central Amazonia? For. Ecol. Manag. 262, 331–338. https://doi.org/10.1016/j.foreco.2011.03.039.

Detto, M., Muller-Landau, H.C., Mascaro, J., Asner, G.P., 2013. Hydrological Networks and Associated Topographic Variation as Templates for the Spatial Organization of Tropical Forest Vegetation. PLoS ONE 8, e76296. https://doi.org/10.1371/journal.pone.0076296.

Di Vittorio, A.V., Negrón-Juárez, R.I., Higuchi, N., Chambers, J.Q., 2014. Tropical forest carbon balance: effects of field- and satellite-based mortality regimes on the dynamics and the spatial structure of Central Amazon forest biomass. Environ. Res. Lett. 9, 034010 https://doi.org/10.1088/1748-9326/9/3/034010.

Dubayah, R.O., Sheldon, S.L., Clark, D.B., Hofton, M.A., Blair, J.B., Hurtt, G.C., Chazdon, R.L., 2010. Estimation of tropical forest height and biomass dynamics using lidar remote sensing at La Selva, Costa Rica: FOREST DYNAMICS USING LIDAR. J. Geophys. Res. Biogeosciences 115, n/a-n/a. https://doi.org/10.1029/2009JG000933.

Epron, D., Bosc, A., Bonal, D., Freycon, V., 2006. Spatial variation of soil respiration across a topographic gradient in a tropical rain forest in French Guiana. J. Trop. Ecol. 22, 565–574. https://doi.org/10.1017/S0266467406003415.

Espírito-Santo, F.D.B., Gloor, M., Keller, M., Malhi, Y., Saatchi, S., Nelson, B., Junior, R.C. O., Pereira, C., Lloyd, J., Frolking, S., Palace, M., Shimabukuro, Y.E., Duarte, V., Mendoza, A.M., López-González, G., Baker, T.R., Feldpausch, T.R., Brienen, R.J.W., Asner, G.P., Boyd, D.S., Phillips, O.L., 2015. Size and frequency of natural forest disturbances and the Amazon forest carbon balance. Nat. Commun. 6 https://doi.org/10.1038/ncomms7638.

Ferry, B., Morneau, F., Bontemps, J.-D., Blanc, L., Freycon, V., 2010. Higher treefall rates on slopes and waterlogged soils result in lower stand biomass and productivity in a tropical rain forest: Treefall and biomass in a tropical rain forest. J. Ecol. 98, 106–116. https://doi.org/10.1111/j.1365-2745.2009.01604.x.

ForestPlots.net, Blundo, C., Carilla, J., Grau, R., Malizia, A., Malizia, L., Osinaga-Acosta, O., Bird, M., Bradford, M., Catchpole, D., Ford, A., Graham, A., Hilbert, D., Kemp, J., Laurance, S., Laurance, W., Ishida, F.Y., Marshall, A., Waite, C., Woell, H., Bastin, J.-F., Bauters, M., Beeckman, H., Boeckx, P., Bogaert, J., De Canniere, C., de Haulleville, T., Doucet, J.-L., Hardy, O., Hubau, W., Kearsley, E., Verbeeck, H., Vleminckx, J., Brewer, S.W., Alarcón, A., Araujo-Murakami, A., Arets, E., Arroyo, L., Chavez, E., Fredericksen, T., Villaroel, R.G., Sibauty, G.G., Killeen, T., Licona, J.C., Lleigue, J., Mendoza, C., Murakami, S., Gutierrez, A.P., Pardo, G., Peña-Claros, M., Poorter, L., Toledo, M., Cayo, J.V., Viscarra, L.J., Vos, V., Ahumada, J., Almeida, E., Almeida, J., de Oliveira, E.A., da Cruz, W.A., de Oliveira, A.A., Carvalho, Fabrício Alvim, Obermuller, F.A., Andrade, A., Carvalho, Fernanda Antunes, Vieira, S.A., Aquino, A.C., Aragão, L., Araújo, A.C., Assis, M.A., Gomes, J.A.M.A., Baccaro, F., de Camargo, P.B., Barni, P., Barroso, J., Bernacci, L.C., Bordin, K., de Medeiros, M.B., Broggio, I., Camargo, J.L., Cardoso, D., Carniello, M.A., Rochelle, A.L.C., Castilho, C., Castro, A.A.J.F., Castro, W., Ribeiro, S.C., Costa, F., de Oliveira, Fernando, R.C., Coutinho, I., Cunha, J., da Costa, L., da Costa Ferreira, L., da Costa Silva, R., da Graça Zacarias Simbine, M., de Andrade Kamimura, V., de Lima, H.C., de Oliveira Melo, L., de Queiroz, L., de Sousa Lima, J.R., do Espírito Santo, M., Domingues, T., dos Santos Prestes, N.C., Carneiro, S.E.S., Elias, F., Eliseu, G., Emilio, T., Farrapo, C.L., Fernandes, L., Ferreira, G., Ferreira, J., Ferreira, L., Ferreira, S., Simon, M.F., Freitas, M.A., García, Q.S., Manzatto, A.G., Graça, P., Guilherme, F., Hase, E., Higuchi, N., Iguatemy, M., Barbosa, R.I., Jaramillo, M., Joly, C., Klipel, J., do Amaral, I.L., Levis, C., Lima, A.S., Dan, M.L., Lopes, A., Madeiros, H., Magnusson, W.E., dos Santos, R. M., Marimon, B., Junior, B.H.M., Grillo, R.M.M., Martinelli, L., Reis, S.M., Medeiros, S., Meira-Junior, M., Metzker, T., Morandi, P., do Nascimento, N.M., Moura, M., Müller, S.C., Nagy, L., Nascimento, H., Nascimento, M., Lima, A.N., de Araújo, R.O., Silva, J.O., Pansonato, M., Sabino, G.P., de Abreu, K.M.P., Rodrigues, P.J.F.P., Piedade, M., Rodrigues, D., Rodrigues Pinto, J.R., Quesada, C., Ramos, E., Ramos, R., Rodrigues, P., de Sousa, T.R., Salomão, R., Santana, F., Scaranello, M., Bergamin, R. S., Schietti, J., Schöngart, J., Schwartz, G., Silva, N., Silveira, M., Seixas, C.S., Simbine, M., Souza, A.C., Souza, P., Souza, R., Sposito, T., Junior, E.S., do Vale, J.D., Vieira, I.C.G., Villela, D., Vital, M., Xaud, H., Zanini, K., Zartman, C.E., Ideris, N.K.H., Metali, F. binti H., Salim, K.A., Saparudin, M.S., Serudin, R.M., Sukri, R.S., Begne, S., Chuyong, G., Djuikouo, M.N., Gonmadje, C., Simo-Droissart, M., Sonké, B., Taedoumg, H., Zemagho, L., Thomas, S., Baya, F., Saiz, G., Espejo, J.S., Chen, D., Hamilton, A., Li, Y., Luo, T., Niu, S., Xu, H., Zhou, Z., Álvarez-Dávila, E., Escobar, J. C.A., Arellano-Peña, H., Duarte, J.C., Calderón, J., Bravo, L.M.C., Cuadrado, B., Cuadros, H., Duque, A., Duque, L.F., Espinosa, S.M., Franke-Ante, R., García, H., Gómez, A., González-M., R., Idárraga-Piedrahíta, Á., Jimenez, E., Jurado, R., Oviedo, W.L., López-Camacho, R., Cruz, O.A.M., Polo, I.M., Paky, E., Pérez, K., Pijachi, A., Pizano, C., Prieto, A., Ramos, L., Correa, Z.R., Richardson, J., Rodríguez, E., Rodriguez M., G.M., Rudas, A., Stevenson, P., Chudomelová, M., Dancak, M., Hédl, R., Lhota, S., Svatek, M., Mukinzi, J., Ewango, C., Hart, T., Yakusu, E.K., Lisingo, J., Makana, J.-R., Mbayu, F., Toirambe, B., Mukendi, J.T., Kvist, L., Nebel, G., Báez, S., Céron, C., Griffith, D.M., Andino, J.E.G., Neill, D., Palacios, W., Peñuela-Mora, M.C., Rivas-Torres, G., Villa, G., Demissie, S., Gole, T., Gonfa, T., Ruokolainen, K., Baisie, M., Bénédet, F., Betian, W., Bezard, V., Bonal, D., Chave, J., Droissart, V., Gourlet-Fleury, S., Hladik, A., Labrière, N., Naisso, P., Réjou-Méchain, M., Sist, P., Blanc, L., Burban, B., Derroire, G., Dourdain, A., Stahl, C., Bengone, N.N., Chezeaux, E., Ondo, F.E., Medjibe, V., Mihindou, V., White, L., Culmsee, H., Rangel, C.D., Horna, V., Wittmann, F., Adu-Bredu, S., Affum-Baffoe, K., Foli, E., Balinga, M., Roopsind, A., Singh, J., Thomas, R., Zagt, R., Murthy, I.K., Kartawinata, K., Mirmanto, E., Priyadi, H., Samsoedin, I., Sunderland, T., Yassir, I., Rovero, F., Vinceti, B., Hérault, B., Aiba, S.-I., Kitayama, K., Daniels, A., Tuagben, D., Woods, J.T., Fitriadi, M., Karolus, A., Khoon, K.L., Majalap, N., Maycock, C., Nilus, R., Tan, S., Sitoe, A., Coronado G., I., Ojo, L., de Assis, R., Poulsen, A.D., Sheil, D., Pezo, K.A., Verde, H.B., Moscoso, V.C., Oroche, J.C.C., Valverde, F.C., Medina, M.C., Cardozo, N.D., de Rutte Corzo, J., del

Aguila Pasquel, J., Llampazo, G.F., Freitas, L., Cabrera, D.G., Villacorta, R.G., Cabrera, K.G., Soria, D.G., Saboya, L.G., Rios, J.M.G., Pizango, G.H., Coronado, E.H., Huamantupa-Chuquimaco, I., Huasco, W.H., Aedo, Y.T.H., Peña, J.L.M., Mendoza, A.M., Rodriguez, V.M., Vargas, P.N., Ramos, S.C.P., Camacho, N.P., Cruz, A.P., Arevalo, F.R., Huaymacari, J.R., Rodriguez, C.R., Paredes, M.A.R., Bayona, L.R., del Pilar Rojas Gonzales, R., Peña, M.E.R., Revilla, N.S., Shareva, Y.C.S., Trujillo, R.T., Gamarra, L.V., Martinez, R.V., Arenas, J.V., Amani, C., Ifo, S.A., Bocko, Y., Boundja, P., Ekoungoulou, R., Hockemba, M., Nzala, D., Fofanah, A., Taylor, D., Bañares-de Dios, G., Cayuela, L., la Cerda, Í.G., Macía, M., Stropp, J., Playfair, M., Wortel, V., Gardner, T., Muscarella, R., Priyadi, H., Rutishauser, E., Chao, K.-J., Munishi, P., Bánki, O., Bongers, F., Boot, R., Fredriksson, G., Reitsma, J., ter Steege, H., van Andel, T., van de Meer, P., van der Hout, P., van Nieuwstadt, M., van Ulft, B., Veenendaal, E., Vernimmen, R., Zuidema, P., Zwerts, J., Akite, P., Bitariho, R., Chapman, C., Gerald, E., Leal, M., Mucunguzi, P., Abernethy, K., Alexiades, M., Baker, T.R., Banda, K., Banin, L., Barlow, J., Bennett, A., Berenguer, E., Berry, N., Bird, N.M., Blackburn, G.A., Brearley, F., Brienen, R., Burslem, D., Carvalho, L., Cho, P., Coelho, F., Collins, M., Coomes, D., Cuni-Sanchez, A., Dargie, G., Dexter, K., Disney, M., Draper, F., Duan, M., Esquivel-Muelbert, A., Ewers, R., Fadrique, B., Fauset, S., Feldpausch, T.R., França, F., Galbraith, D., Gilpin, M., Gloor, E., Grace, J., Hamer, K., Harris, D., Jeffery, K., Jucker, T., Kalamandeen, M., Klitgaard, B., Levesley, A., Lewis, S.L., Lindsell, J., Lopez-Gonzalez, G., Lovett, J., Malhi, Y., Marthews, T., McIntosh, E., Melgaço, K., Milliken, W., Mitchard, E., Moonlight, P., Moore, S., Morel, A., Peacock, J., Peh, K.S.-H., Pendry, C., Pennington, R.T., de Oliveira Pereira, L., Peres, C., Phillips, O.L., Pickavance, G., Pugh, T., Qie, L., Riutta, T., Roucoux, K., Ryan, C., Sarkinen, T., Valeria, C.S., Spracklen, D., Stas, S., Sullivan, M., Swaine, M., Talbot, J., Taplin, J., van der Heijden, G., Vedovato, L., Willcock, S., Williams, M., Alves, L., Loayza, P.A., Arellano, G., Asa, C., Ashton, P., Asner, G., Brncic, T., Brown, F., Burnham, R., Clark, C., Comiskey, J., Damasco, G., Davies, S., Di Fiore, T., Erwin, T., Farfan-Rios, W., Hall, J., Kenfack, D., Lovejoy, T., Martin, R., Montiel, O.M., Pipoly, J., Pitman, N., Poulsen, J., Primack, R., Silman, M., Steininger, M., Swamy, V., Terborgh, J., Thomas, D., Umunay, P., Uriarte, M., Torre, E.V., Wang, O., Young, K., Aymard C., G.A., Hernández, L., Fernández, R.H., Ramírez-Angulo, H., Salcedo, P., Sanoja, E., Serrano, J., Torres-Lezama, A., Le, T.C., Le, T.T., Tran, H.D., 2021. Taking the pulse of Earth's tropical forests using networks of highly distributed plots. Biol. Conserv. 260, 108849. 10.1016/j. biocon.2020.108849.

Gale, N., 2006. The Relationship between Canopy Gaps and Topography in a Western Ecuadorian Rain Forest1. Biotropica 32, 653–661. https://doi.org/10.1111/j.1744-7429.2000.tb00512.x.

Gourlet-Fleury, S. (ed), Guehl, J.-M. (ed), Laroussinie, O. (ed), 2004. Ecology and management of a neotropical rainforest : lessons drawn from Paracou, a long-term experimental research site in French Guiana. Elsevier.

Harms, K.E., Condit, R., Hubbell, S.P., Foster, R.B., 2001. Habitat associations of trees and shrubs in a 50-ha neotropical forest plot: *Habitat associations of trees and shrubs*. J. Ecol. 89, 947–959. https://doi.org/10.1111/j.1365-2745.2001.00615.x.

Hijmans, R.J., 2020. raster: Geographic Data Analysis and Modeling.

Hunter, M.O., Keller, M., Morton, D., Cook, B., Lefsky, M., Ducey, M., Saleska, S., de Oliveira, R.C., Schietti, J., 2015. Structural Dynamics of Tropical Forest Gaps. PLoS ONE 10, e0132144. https://doi.org/10.1371/journal.pone.0132144.

IPCC, In Press. Summary for Policymakers. In: Climate Change 2021: The Physical Science Basis. Contribution of Working Group I to the Sixth Assessment Report of the Intergovernmental Panel on Climate Change.

Kellner, J.R., Asner, G.P., 2009. Convergent structural responses of tropical forests to diverse disturbance regimes. Ecol. Lett. 12, 887–897. https://doi.org/10.1111/j.1461-0248.2009.01345.x.

Kohyama, T.S., Kohyama, T.I., Sheil, D., 2018. Definition and estimation of vital rates from repeated censuses: Choices, comparisons and bias corrections focusing on trees. Methods Ecol. Evol. 9, 809–821. https://doi.org/10.1111/2041-210X.12929.

Laurance, W.F., Williamson, G.B., 2001. Positive Feedbacks among Forest Fragmentation, Drought, and Climate Change in the Amazon. Conserv. Biol. 15, 1529–1535. https://doi.org/10.1046/j.1523-1739.2001.01093.x.

Leitold, V., Morton, D.C., Longo, M., dos-Santos, M.N., Keller, M., Scaranello, M., 2018. El Niño drought increased canopy turnover in Amazon forests. New Phytol. 219, 959–971. https://doi.org/10.1111/nph.15110.

Longo, M., Saatchi, S., Keller, M., Bowman, K., Ferraz, A., Moorcroft, P.R., Morton, D.C., Bonal, D., Brando, P., Burban, B., Derroire, G., dos-Santos, M.N., Meyer, V., Saleska, S., Trumbore, S., Vincent, G., 2020. Impacts of Degradation on Water, Energy, and Carbon Cycling of the Amazon Tropical Forests. J. Geophys. Res. Biogeosciences 125. 10.1029/2020JG005677.

Malhi, Y., Phillips, O.L., Lloyd, J., Baker, T., Wright, J., Almeida, S., Arroyo, L., Frederiksen, T., Grace, J., Higuchi, N., Killeen, T., Laurance, W.F., Leaño, C., Lewis, S., Meir, P., Monteagudo, A., Neill, D., Núñez Vargas, P., Panfil, S.N., Patiño, S., Pitman, N., Quesada, C.A., Rudas-Ll., A., Salomão, R., Saleska, S., Silva, N., Silveira, M., Sombroek, W.G., Valencia, R., Vásquez Martínez, R., Vieira, I.C.G., Vinceti, B., 2002. An international network to monitor the structure, composition and dynamics of Amazonian forests (RAINFOR). J. Veg. Sci. 13, 439–450. 10.1111/j.1654-1103.2002.tb02068.x.

Malhi, Y., Roberts, J.T., Betts, R.A., Killeen, T.J., Li, W., Nobre, C.A., 2008. Climate Change, Deforestation, and the Fate of the Amazon. Science 319, 169–172. https://doi.org/10.1126/science.1146961.

Marvin, D.C., Asner, G.P., Knapp, D.E., Anderson, C.B., Martin, R.E., Sinca, F., Tupayachi, R., 2014. Amazonian landscapes and the bias in field studies of forest structure and biomass. Proc. Natl. Acad. Sci. 111, E5224–E5232. https://doi.org/10.1073/pnas.1412999111.

Mattivi, P., Franci, F., Lambertini, A., Bitelli, G., 2019. TWI computation: a comparison of different open source GISs. Open Geospatial Data Softw. Stand. 4, 6. https://doi.org/10.1186/s40965-019-0066-y.

McDowell, N., Allen, C.D., Anderson-Teixeira, K., Brando, P., Brienen, R., Chambers, J., Christoffersen, B., Davies, S., Doughty, C., Duque, A., Espirito-Santo, F., Fisher, R., Fontes, C.G., Galbraith, D., Goodsman, D., Grossiord, C., Hartmann, H., Holm, J., Johnson, D.J., Kassim, Abd.R., Keller, M., Koven, C., Kueppers, L., Kumagai, T., Malhi, Y., McMahon, S.M., Mencuccini, M., Meir, P., Moorcroft, P., Muller-Landau, H.C., Phillips, O.L., Powell, T., Sierra, C.A., Sperry, J., Warren, J., Xu, C., Xu, X., 2018. Drivers and mechanisms of tree mortality in moist tropical forests. New Phytol. 219, 851–869. 10.1111/nph.15027.

Meyer, V., Saatchi, S.S., Chave, J., Dalling, J.W., Bohlman, S., Fricker, G.A., Robinson, C., Neumann, M., Hubbell, S., 2013. Detecting tropical forest biomass dynamics from repeated airborne lidar measurements. Biogeosciences 10, 5421–5438. https://doi.org/10.5194/bg-10-5421-2013.

Morneau, F., 2007. Effets d'un gradient d'engorgement sur la structure et la dynamique d'une forêt tropicale humide (Paracou, Guyane française) (Theses). ENGREF (AgroParisTech).

Pan, Y., Birdsey, R.A., Fang, J., Houghton, R., Kauppi, P.E., Kurz, W.A., Phillips, O.L., Shvidenko, A., Lewis, S.L., Canadell, J.G., Ciais, P., Jackson, R.B., Pacala, S.W., McGuire, A.D., Piao, S., Rautiainen, A., Sitch, S., Hayes, D., 2011. A Large and Persistent Carbon Sink in the World's Forests. Science 333, 988–993. https://doi.org/10.1126/science.1201609.

Parent, C., Nicolas, C., Audrey, B., Crevècoeur, M., Dat, J., 2008. An overview of plant responses to soil waterlogging. Plant Stress 20–27.

Pélissier, R., Dray, S., Sabatier, D., 2002. Within-plot relationships between tree species occurrences and hydrological soil constraints: an example in French Guiana investigated through canonical correlation analysis. Plant Ecol. 162, 143–156. https://doi.org/10.1023/A:1020399603500.

Phillips, O.L., Lewis, S.L., Baker, T.R., Chao, K.-J., Higuchi, N., 2008. The changing Amazon forest. Philos. Trans. R. Soc. B Biol. Sci. 363, 1819–1827. https://doi.org/10.1098/rstb.2007.0033.

Phillips, O.L., Lewis, S.L., Higuchi, N., Baker, T., 2016. Recent Changes in Amazon Forest Biomass and Dynamics, in: Nagy, L., Forsberg, B.R., Artaxo, P. (Eds.), Interactions Between Biosphere, Atmosphere and Human Land Use in the Amazon Basin, Ecological Studies. Springer Berlin Heidelberg, Berlin, Heidelberg, pp. 191–224. 10.1007/978-3-662-49902-3_10.

Réjou-Méchain, M., Barbier, N., Couteron, P., Ploton, P., Vincent, G., Herold, M., Mermoz, S., Saatchi, S., Chave, J., de Boissieu, F., Féret, J.-B., Takoudjou, S.M., Pélissier, R., 2019. Upscaling Forest Biomass from Field to Satellite Measurements: Sources of Errors and Ways to Reduce Them. Surv. Geophys. 40, 881–911. https://doi.org/10.1007/s10712-019-09532-0.

Rex, F.E., Corte, A.P.D., Silva, C.A., Machado, S.A., Sanquetta, C.R., 2020. Dynamics of Above-Ground Biomass in the Brazilian Amazon Using LiDAR Data. Anuário Inst. Geociências - UFRJ 43, 228–238. https://doi.org/10.11137/2020_1_228_238.

Roussel, J.-R., Auty, D., 2020. lidR: Airborne LiDAR Data Manipulation and Visualization for Forestry Applications.

Roussel, J.-R., Caspersen, J., Béland, M., Thomas, S., Achim, A., 2017. Removing bias from LiDAR-based estimates of canopy height: Accounting for the effects of pulse density and footprint size. Remote Sens. Environ. 198, 1–16. https://doi.org/10.1016/j.rse.2017.05.032.

Schmitt, L., 1984. Recherches sylvicoles sur les peuplements naturels en forêt dense guyanaise. Phase préliminaire : localisation du dispositif principal. Nogent-sur-Marne, GERDAT-CTFT. ed.

Senécal, J.-F., Doyon, F., Messier, C., 2018. Tree Death Not Resulting in Gap Creation: An Investigation of Canopy Dynamics of Northern Temperate Deciduous Forests. Remote Sens. 10, 121. https://doi.org/10.3390/rs10010121.

Sousa, T.R., Schietti, J., Coelho de Souza, F., Esquivel-Muelbert, A., Ribeiro, I.O., Emílio, T., Pequeno, P.A.C.L., Phillips, O., Costa, F.R.C., 2020. Palms and trees resist extreme drought in Amazon forests with shallow water tables. J. Ecol. 108, 2070–2082. https://doi.org/10.1111/1365-2745.13377.

Thomas, R.Q., Kellner, J.R., Clark, D.B., Peart, D.R., 2013. Low mortality in tall tropical trees. Ecology 94, 920–929. https://doi.org/10.1890/12-0939.1.

van der Meer, P.J., Bongers, F., 1996. Patterns of Tree-Fall and Branch-Fall in a Tropical Rain Forest in French Guiana. J. Ecol. 84, 19–29. https://doi.org/10.2307/2261696.

Vieira, S., de Camargo, P.B., Selhorst, D., da Silva, R., Hutyra, L., Chambers, J.Q., Brown, I.F., Higuchi, N., dos Santos, J., Wofsy, S.C., Trumbore, S.E., Martinelli, L.A., 2004. Forest structure and carbon dynamics in Amazonian tropical rain forests. Oecologia 140, 468–479. https://doi.org/10.1007/s00442-004-1598-z.

Vincent, G., Antin, C., Laurans, M., Heurtebize, J., Durrieu, S., Lavalley, C., Dauzat, J., 2017. Mapping plant area index of tropical evergreen forest by airborne laser scanning. A cross-validation study using LAI2200 optical sensor. Remote Sens. Environ. 198, 254–266. https://doi.org/10.1016/j.rse.2017.05.034.

Vincent, G., Sabatier, D., Blanc, L., Chave, J., Weissenbacher, E., Pélissier, R., Fonty, E., Molino, J.-F., Couteron, P., 2012. Accuracy of small footprint airborne LiDAR in its predictions of tropical moist forest stand structure. Remote Sens. Environ. 125, 23–33. https://doi.org/10.1016/j.rse.2012.06.019.

Vincent, G., Sabatier, D., Rutishauser, E., 2014. Revisiting a universal airborne light detection and ranging approach for tropical forest carbon mapping: scaling-up from tree to stand to landscape. Oecologia 175, 439–443. https://doi.org/10.1007/s00442-014-2913-y.

Vincent, G., Weissenbacher, E., Sabatier, D., Blanc, L., Proisy, C., Couteron, P., 2010. Détection des variations de structure de peuplements en forêt dense tropicale humide par Lidar aéroporté. Rev. Francaise Photogramm. Teledetection.

Xiao, J., Chevallier, F., Gomez, C., Guanter, L., Hicke, J.A., Huete, A.R., Ichii, K., Ni, W., Pang, Y., Rahman, A.F., Sun, G., Yuan, W., Zhang, L., Zhang, X., 2019. Remote

sensing of the terrestrial carbon cycle: A review of advances over 50 years. Remote Sens. Environ. 233, 111383 https://doi.org/10.1016/j.rse.2019.111383.